2019

Miniaturization of higher order mode circular microstrip patch antennas

Saininad Chandrakant Naik

MINIATURIZATION OF HIGHER ORDER

MODE CIRCULAR MICROSTRIP PATCH

ANTENNAS

by

SAININAD CHANDRAKANT NAIK

A THESIS

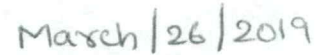Submitted in partial fulfillment of the requirements
for the degree of Master of Science
in
The Department of Electrical and Computer Engineering
to
The School of Graduate Studies
of
The University of Alabama in Huntsville

HUNTSVILLE, ALABAMA
2019

In presenting this thesis in partial fulfillment of the requirements for a master's degree from The University of Alabama in Huntsville, I agree that the Library of this University shall make it freely available for inspection. I further agree that permission for extensive copying for scholarly purposes may be granted by my advisor or, in his/her absence, by the Chair of the Department or the Dean of the School of Graduate Studies. It is also understood that due recognition shall be given to me and to The University of Alabama in Huntsville in any scholarly use which may be made of any material in this thesis.

_____   March / 26 / 2019
(Saininad Chandrakant Naik)   (Date)

THESIS APPROVAL FORM

Submitted by Saininad Chandrakant Naik in partial fulfillment of the requirements for the degree of Master of Science in Electrical Engineering and accepted on behalf of the Faculty of the School of Graduate Studies by the thesis by the committee.

We, the undersigned members of the Graduate Faculty of The University of Alabama in Huntsville, certify that we have advised and/or supervised the candidate on the work described in this thesis. We further certify that we have reviewed the thesis manuscript and approve it in partial fulfillment of the requirements for the degree of Master of Science in Electrical and Computer Engineering.

_____ 3/26/2019 Committee Chair
Dr. Maria Pour   (Date)

_____ 3/14/2019
Dr. Tony Gatlin   (Date)

_____ 3/14/2019
Dr. David Pan   (Date)

_____ 3/27/19
Dr. Ravi Gorur   (Date)

_____ 04/01/19 College Dean
Dr. Shankar Mahalingam   (Date)

_____ 4/9/19   Graduate Dean
Dr. David Berkowitz   (Date)

ABSTRACT
School of Graduate Studies
The University of Alabama in Huntsville

Degree: <u>Master of Science in Engineering</u>   Dept.: <u>Electrical and Computer Engineering</u>

Name of candidate: <u>Saininad Chandrakant Naik</u>

Title   <u>Miniaturization of Higher Order Mode Circular Microstrip Patch Antennas</u>

Microstrip patch antennas operating at higher order modes are suitable for applications in satellite communications, global positioning systems and anti-jamming systems. Such antennas are capable of generating conical radiation patterns when excited at certain higher order modes, making them excellent candidates for satellite systems, especially for lower elevation angles. However, the radius of circular patch antennas increases, as higher order modes are excited, which has hindered its applications in tightly-space antenna and array configurations. More specifically, based on the cavity model the patch radii are proportionally related to the eigenvalues of the equivalent cavity enclosing the patch, corresponding to the zeros of the derivative of Bessel functions of first kind. The modes of interest in this thesis are the TM_{21} and TM_{31} modes, generating conical patterns as well as the TM_{12} mode, producing broadside radiation patterns. The thesis is focused on reducing the eigenvalues of the TM_{21} and TM_{31} higher modes close to that of the dominant mode, as well as decreasing the resonant frequency of the TM_{12} mode. Herein, the proposed miniaturization is realized by a proper geometrical alteration in the patch layer which is inspired by associated surface current distributions of the aforementioned modes. As for the TM_{12} mode, which inherently has unwanted sidelobes in one of the principal planes, attempts are made to simultaneously reduce its resonant frequency to realize a dual-band antenna and obliterate the undesired sidelobes.

Abstract Approval: Committee Chair _____

Department Chair _____

Graduate Dean _____

ACKNOWLEDGEMENTS

I would like to express my sincere gratitude and appreciation to my advisor and committee chair Dr. Maria Pour for giving me this opportunity to perform research under her guidance. Her experience, unparalleled support and profound belief in my abilities inspired me to explore my potential and handle challenges with ease.

I would like to convey my deepest appreciation to my committee members, Dr. Tony Gatlin and Dr. David Pan for devoting their time to reviewing this thesis and advising me with valuable suggestions.

I am grateful to God to have blessed me with caring and supportive parents. Thank you for teaching me that my job in life is to learn, to be happy, and to know and understand myself, only then could I know and understand others. I would like to extend my gratitude to my family and friends in India who have provided me with emotional support and encouragement.

Lastly, I would like to thank Bhagwan Sri Satya Sai Baba for giving me the strength to go after my dreams.

TABLE OF CONTENTS

LIST OF FIGURES

LIST OF TABLES

LIST OF SYMBOLS

ε_r *Relative permittivity of the material*

ε_{eff} *Effective permittivity of the medium*

λ_o *Wavelength in free space*

λ_d *Wavelength in a medium*

κ_o *Wave number*

η *Intrinsic impedance*

θ *Elevation angle*

ϕ *Azimuth angle*

CHAPTER 1

Introduction

1.1 Preface

IEEE defines an antenna as "That part of a transmitting or receiving system that is designed to radiate or to receive electromagnetic waves" [1]. An antenna acts as a transducer, facilitating the conversion of electric currents and voltages to electromagnetic waves and vice versa. Antennas came into existence to support the military needs in the late 19th century. In successive decades, they were employed for commercial purposes such as telephone and radio services. Since then, research has been conducted to design antennas with their rising applications for the telecommunication, military, and commercial purposes.

To facilitate a wireless communication link between two systems, antennas are needed to transmit and receive signals. Different applications brought challenges to the design of antennas. Over the years, various types of antennas have been designed to meet specific requirements. For example, parabolic reflector antennas are preferred for high-gain satellite and space applications. In contrast, light-weight and compact antennas, such as microstrip patch antennas, are much preferred in mobile wireless communication systems. Over the years, the ever-increasing demands for higher data rates and versatile communication channels have driven antenna engineers to develop multi-function and compact antennas that can easily be adapted with the growing needs in modern wireless

systems. In compact wireless units, for example, miniaturized and small antennas are needed, which is the main focus of this research.

As of now, microstrip patch antennas are one of the most prominently used antennas, as they are low profile, lightweight, and cost-effective [2]. Their applications range from satellite communications and military requirements to cellular and portable wireless communications. The antenna characteristics such as gain, polarization, radiation patterns, impedance, and bandwidth can be controlled by altering the dimension and design of the patch antenna. Different feeding mechanisms can be used to excite the patch antennas, namely probe feed, microstrip line feed, proximity feed, and aperture coupling feed [3]. A microstrip patch antenna excited at its dominant mode is commonly used in mobile wireless communication systems, as it is compact in size and can readily be conformed to both planar and curved platforms. Depending on the operating mode, microstrip patch antennas produce different radiation patterns. In particular, when excited at the Transverse Magnetic TM_{n1} modes, they generate broadside and conical radiation patterns for n=1 and all other integers of n>1, respectively. In particular, the TM_{n1} modes with n>1 radiate efficiently at low elevation angles, thus making patch antennas suitable for satellites at the horizon. Such multimode microstrip patch antennas are useful in Global Positioning System (GPS) and satellite systems [4]. Apart from the various advantages offered by microstrip patch antennas, antenna designers face challenges such as impedance matching, narrow bandwidth, unwanted sidelobes in radiation patterns, and poor cross polarization discriminations [3]. There has been growing research to address these limitations, while maintaining the antenna dimensions as small as possible.

1.2 Motivation

As mentioned in Section 1.1, microstrip patch antennas have become an integral part of wireless communication systems because of their distinct advantages. Recent advancements in compact and mobile wireless communication systems necessitate the need to design compact and miniaturized antennas. Many compact antennas with enhanced gain, dual-frequency operation, improved polarization purity, and wideband characteristics have been reported in the literature. However, the main emphasis has been placed on microstrip patch antennas with broadside radiation patterns, excited at their dominant mode. Due to the attractive features of the higher order mode patch antennas, which are capable of generating conical patterns well suited for wireless applications in off-boresight communications, an investigation is undertaken here to miniaturize patch antennas at their higher order modes. The main drawback of higher mode antennas is that they need a much larger patch size, compared to their dominant-mode counterparts, to resonate at a given frequency.

The motivation of this study derives from the need to design cost-effective patch antennas excited at higher modes with miniaturized and compact patch sizes, comparable to the one operating at the dominant mode at a given frequency. The potential challenges faced on miniaturizing higher mode antennas are discussed in the following chapter along with a review on compact, cost-effective higher mode patch antennas.

1.3 Research Objective

The research presented in this thesis focuses on the miniaturization of higher mode circular patch antennas to be used as an element in scanning phased array configurations. The following steps define the scope of the research presented in this thesis:

- Miniaturization of the TM_{21} circular patch antenna with conical radiation patterns using the full-wave electromagnetic solver [31], especially reducing the eigenvalue of the TM_{21} mode to that of the dominant mode. Verifying the numerical results by testing a prototype of the fabricated antenna.

- Numerically investigating the miniaturization of the TM_{31} circular patch antenna with conical radiation patterns and reducing the TM_{31} mode eigenvalue close to the eigenvalue of the dominant mode.

- Study a dual-band circular patch antenna with a low frequency ratio and identical broadside radiation patterns with no sidelobes.

1.4 Structure of the Thesis

In this thesis, research was conducted to miniaturize the higher mode circular microstrip patch antennas close to the size of the dominant mode. The research objective and the motive behind the research topic are explained in this chapter.

Chapter 2 describes the background theory and a literature review on circular microstrip patch antennas. The cavity model will be explained and the general equations governing the model will be provided. A review of some miniaturization techniques will

also be provided in Chapter 2, followed by some existing challenges in developing miniaturized antennas.

Chapter 3 presents the methodology to design the TM_{21} circular patch antenna. A new antenna design is put forth to reduce the area occupied by the patch operating at the TM_{21} mode to that of the dominant mode. A parametric study is conducted on the proposed antenna. The designed antenna is fabricated and tested in an anechoic chamber.

In Chapter 4, a miniaturized TM_{31} circular microstrip patch antenna is designed. A parametric study is conducted to understand the miniaturization impact on the frequency and radiation characteristics of the antenna.

In Chapter 5, a dual-band circular patch antenna will be investigated. The newly designed antenna upholds the characteristics of dual-band antennas such as identical radiation patterns and almost similar polarization on the patch. The research focuses on realizing a small frequency ratio for this dual-band antenna. An extensive parametric study is conducted to finalize the design.

Culminating the thesis, the closing chapter presents the concluding remarks and summarizes the results of all the research undertaken in the thesis. A future scope of work is also briefed in Chapter 6.

CHAPTER 2

Literature Review and Background Theory

2.1 Introduction

Microstrip patch antennas were first proposed by Deschamps in 1953 [5] and took shape in the mid-1970s [6]. Microstrip patch antennas are well known for their lightweight, small profile and inexpensive fabrication compared to other types of antennas. The size and shape of the microstrip patch and the dielectric substrate determine the resonant frequency, radiation patterns, and other characteristics. The adaptive features of microstrip patch antennas make them suitable for numerous applications such as satellite communication, anti-jamming, and phased array applications in radar. However, microstrip patch antennas have some drawbacks, including narrow bandwidth, low gain, and polarization impurity.

A microstrip patch antenna comprises of three regions, namely the radiating patch, the dielectric substrate, and the ground plane. The dielectric substrate is placed between the radiating patch and the ground plane and provides mechanical support to the antenna. The ground plane reduces the unwanted back lobe in the radiation pattern. The patch size determines the resonant frequency and also controls the operating mode. In general, a microstrip patch antenna supported by a thin grounded dielectric slab excites the transverse magnetic modes, i.e. TM_{nm} modes, due to fact that electric fields are mainly perpendicular to the patch [7]. A circular microstrip patch antenna generates a broadside radiation pattern, when excited at its dominant mode. Certain higher order modes, such as the TM_{n1} with

$n\neq1$, produce conical radiation patterns with a null at the boresight direction of $\theta = 0^\circ$, which are useful for anti-jamming applications [7]. As the mode index number n increases, the main beam of the antenna moves farther away from the boresight direction of $\theta=0^\circ$, making the antenna well suited for communications with satellites at the horizon. However, the drawback of using higher order modes is that the required aperture area is much greater than the dominant mode.

2.2 Background Theory on Circular Microstrip Patch Antennas

Microstrip patch antennas came into commercial use in the 1970s with the development of photo-lithography fabrication techniques, along with dielectric substrates with low loss tangent. The low-cost fabrication and easy integration of patch antennas with microwave circuits contributed to their wide usage in multitudinous applications, such as mobile wireless systems, satellite communications, marine radar, medicine and surveillance radar to name a few. Over the years, immense research has been conducted to overcome the limitations of microstrip antennas such as low efficiency, narrow frequency bandwidth, and poor scanning performance.

The radiating patch of a microstrip antenna can assume any shape, however, well-defined geometrical shapes are preferred such as rectangle, square, circle, etc. The circular patch is preferred over other shapes. The radiation function of circular patch antennas is the product of two independent mathematical functions of azimuth and elevation angles, thus facilitating controlling the radiation patterns in the aforementioned angular ranges. The far-field equations of circular microstrip patch antennas can be determined using three models, including the cavity model, the transmission model, and the full wave model [7]. The cavity model is favored as it is more accurate than the transmission model and less

complex than the full wave model [2]. In the cavity model, the volume confined between the radiating patch and the ground plane is considered as a cavity, surrounded by a peripheral magnetic wall. The top and bottom of the substrate is surrounded by electric walls [7]. Therefore, the fields are uniform along the height of the substrate, provided its thickness is small compared to the operating wavelength, exciting the TM modes. The sum of the resonant modes of the two-dimensional cavity resonator contributes to the fields underneath the patch of the antenna [8].

Due to the finite size of the microstrip patch, the electric field ceases to continue at the periphery creating fringing electric fields. The fringing fields make the electrical dimensions of the patch look larger than its physical dimensions.

2.2.1 Fields and Currents

Typical geometry of a probe-fed circular microstrip patch antenna is shown in Fig. 2.1. The patch and the supporting ground plane are made of perfect electric conductors (PEC). The patch is printed or etched on a thin dielectric slab. The radiating patch is excited by a probe feed, which is placed along the x-axis in Fig. 2.1. As a result, only the transverse magnetic (TM) with respect to the z-axis will be excited, whose electromagnetic fields inside the cavity are obtained by solving the wave equation in the cylindrical coordinates and satisfying the proper boundary conditions in the cavity. The fields inside the cavity are given by,

$$E_z = E_0 \left(J_{n+1}(\kappa a) + J_{n-1}(\kappa a)\right) \cos n\phi \qquad (2.1)$$

$$H_\rho = \frac{j}{\omega\mu\rho}\frac{dE_z}{d\phi} = -\frac{jn}{\omega\mu\rho}E_0\left(J_{n+1}(\kappa a) + J_{n-1}(\kappa a)\right)\sin n\phi \qquad (2.2)$$

$$H_\phi = \frac{j}{\omega\mu}\frac{dE_z}{d\rho} = -\frac{j\kappa}{\omega\mu}E_0\left(J_{n+1}(\kappa a) - J_{n-1}(\kappa a)\right)\cos n\phi \qquad (2.3)$$

where k is the propagation constant in the dielectric, ω is the angular frequency, i.e. $\omega = 2\pi f$, J_n is the Bessel function of the first kind and order n, and a is the radius of the patch. E_0 is the strength of the electric field at the edge of the patch. An induced electric current is developed on the inner surface of the radiating patch due to the magnetic fields inside the cavity. The electric surface current J_ρ should vanish at the edges as per the magnetic field boundary condition. Hence, there exists a certain radius, associated with each of the TM modes, which is determined by the zeros of the derivative of the Bessel function [7], as further detailed in the next section.
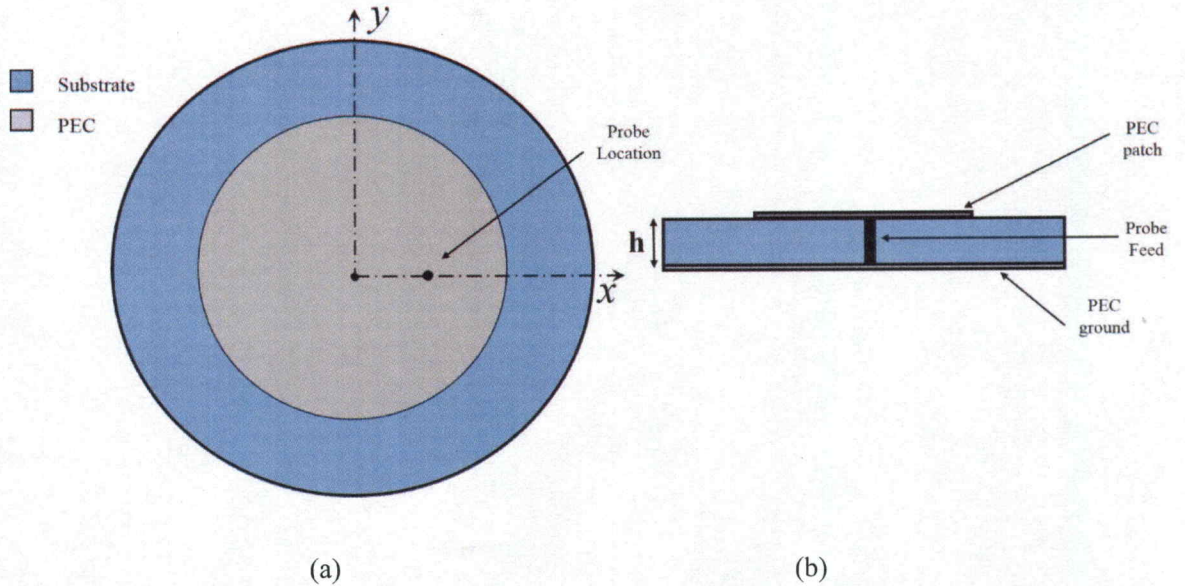
Fig. 2.1: (a) Top view and (b) side view of a typical microstrip patch antenna fed by a 50Ω SMA probe that excites the TM modes.

2.2.2 Resonant Frequencies

The resonant frequencies of different TM$_{nm}$ modes are calculated by equation (2.4) [7].

$$(f_r)_{nm} = \frac{\chi_{nm} C}{2\pi a \sqrt{\varepsilon_{eff}}} \qquad (2.4)$$

χ_{nm}, also known as the eigenvalue, is the mth zero of the derivative of the Bessel function of order n of the first kind and satisfies the magnetic boundary conditions; n and m are the mode index numbers. In Equation (2.4), a is the radius of the radiating patch, C is the speed of light in free space, and ε_{eff} is the effective dielectric constant of the substrate. The first six eigenvalues of χ_{nm} are listed in Table 2.1 [7].

Table 2.1: Roots of derivative of Bessel function for determining the patch radius at different TM modes [7]

Mode	TM$_{11}$	TM$_{21}$	TM$_{02}$	TM$_{31}$	TM$_{41}$	TM$_{12}$
χ_{nm}	1.84118	3.05424	3.83	4.20119	5.317	5.331

2.2.3 Radiation Fields

The E_z field from equation (2.1) is used to derive the equivalent magnetic current, expressed by equation (2.5). The auxiliary electric vector potential is then calculated over the antenna aperture by integrating the derived equivalent magnetic current to determine the radiated electric field in the far-field region, whose θ- and ϕ-components are given by equations (2.6) and (2.7), respectively. This approach of deriving the electric far fields of the antenna is known as the aperture field approach. Equations (2.8) and (2.9) give the final

electric far field expressions for x-polarized waves. These equations are calculated after considering the contribution of only a single mode at a particular frequency [7], assuming an infinite ground plane.

$$\vec{M} = \vec{E} \times \hat{\rho} = E_z \hat{\phi} = \hat{\phi} \sum_{n=0}^{\infty} E_n \frac{(J_{n+1}(\kappa a_{nm}) + J_{n-1}(\kappa a_{nm})) \kappa a_{nm}}{2n} \cos n\phi \tag{2.5}$$

$$E_\theta = \frac{-j\kappa_0}{4\pi} \frac{e^{-j\kappa_0 r}}{r} \int_0^{2\pi} \int_0^\rho M_\phi(\rho, \phi') \cos(\phi' - \phi) \exp[j\kappa_0 \rho \sin\theta \cos(\phi' - \phi)] \rho d\rho d\phi' \tag{2.6}$$

$$E_\phi = \frac{-j\kappa_0}{4\pi} \frac{e^{-j\kappa_0 r}}{r} \cos\theta \int_0^{2\pi} \int_0^\rho M_\theta(\rho, \phi') \sin(\phi'$$
$$- \phi) \exp[j\kappa_0 \rho \sin\theta \cos(\phi' - \phi)] \rho d\rho d\phi' \tag{2.7}$$

$$E_\theta = j^n \frac{V a_{nm} \kappa_0}{4} \frac{e^{-j\kappa_0 r}}{r} \left(J_{n+1}(\kappa a_{nm} \sin(\theta)) - J_{n-1}(\kappa a_{nm} \sin(\theta))\right) \cos n\phi \tag{2.8}$$

$$E_\phi = j^n \frac{V a_{nm} \kappa_0}{4} \frac{e^{-j\kappa_0 r}}{r} \cos\theta \left(J_{n+1}(\kappa a_{nm} \sin(\theta)) + J_{n-1}(\kappa a_{nm} \sin(\theta))\right) \sin n\phi \tag{2.9}$$

where V is the edge voltage along the feed axis and is equal to $h E_n J_n(\chi_{nm})$.

Based on the far-field radiation equations of (2.8) and (2.9), it is clear that the radiation patterns of a microstrip circular patch antennas depend on its operating mode. As mentioned previously, the higher order modes of TM_{n1} with $n \neq 1$ have a conical pattern with a null at the $\theta = 0°$, whereas the dominant TM_{11} mode has a broadside pattern with its main beam at the $\theta = 0°$. Typical radiation patterns of the first three modes in a circular microstrip patch antenna are illustrated in Fig. 2.2 at their respective principal planes [9].
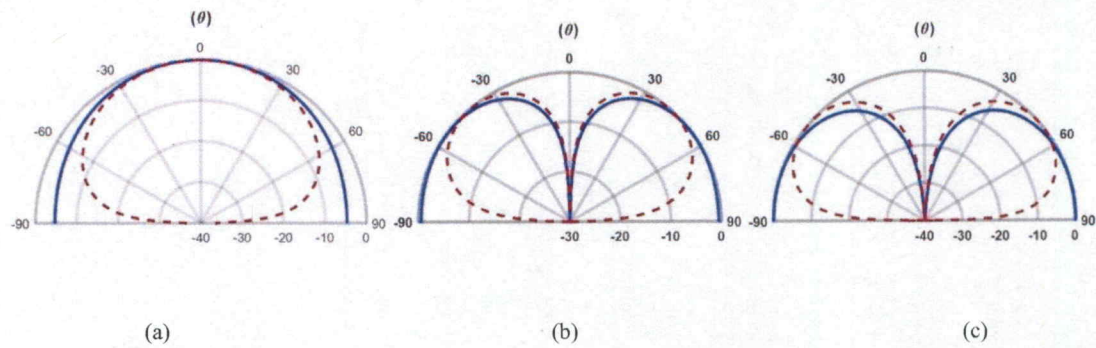
Fig. 2.2: Typical radiation patterns of a circular patch antenna operating at the (a) TM_{11} mode (b) TM_{21} mode (c) TM_{31} mode; E-Plane —— and H-Plane — —

2.3 Physical Limitations on Electrically Small Antennas

A microstrip patch antenna resonating at a specific frequency is designated as 'miniaturized' when the linear dimensions are smaller than the reference patch designed at the same frequency. The miniaturization of an antenna deals with the best compromise in bandwidth, volume, and gain when most of the assigned volume is utilized in the radiation.

The miniaturization of an antenna affects its radiation characteristics, bandwidth, polarization, gain and eventually the efficiency of the antenna. Feeding small antennas also present a different challenge to antenna designers.

In the 1940s, the effect of miniaturization was studied by Wheeler [10] on radiation properties. A ratio between the antenna resistance and antenna reactance was used to define radiation power factor to measure the radiation of an antenna. Wheeler showed that the product of the bandwidth and efficiency is equivalent to the radiation power factor using a simple lumped-circuit model, where the antenna is matched. He confirmed that this product was directly related to the area occupied by the antenna, as the reactance increases with any decrease in size and eventually the radiation resistance becomes small.

12

This work was taken forward by Chu [11], who derived a relation between minimum quality factor, using omnidirectional antennas, and the antenna volume based on an equivalent circuit of lumped elements using the spherical wave impedance functions around the antenna. The computation of the quality factor, i.e. Q, was simplified further in [12-14] and the smallest possible Q for a linearly polarized antenna was given by equation (2.10),

$$Q = \frac{1}{(ka)^3} + \frac{1}{ka} \tag{2.10}$$

Harrington [15] extended the work done by Wheeler and Chu and incorporated the effects of losses. Harrington proposed a straightforward formula to determine the normal gain that a miniaturized antenna can attain having a reasonable bandwidth. Equation (2.11) gives an upper limit for the gain, i.e. G, for small antennas. Electrically small antennas cannot reach the limit as the radiation region of the antenna becomes very small as losses may increase drastically. Nevertheless, the equation stands good for paradigm antennas.

$$G = (ka)^2 + 2(ka) \tag{2.11}$$

The miniaturization of an antenna impacts its bandwidth, efficiency and gain. Apart from these characteristics, miniaturization also has a negative impact on polarization purity. In [16], a planar inverted-F antenna was miniaturized by meandering the surface currents so that the antenna looked electrically larger than its physical size, however it led to unwanted cross-polarized radiation. Lastly, feeding an electrically small antenna becomes challenging in practice. The overall size of the microstrip patch antenna also depends on the size of the ground plane. As the size of the ground plane is cut down as a result of miniaturization, it becomes a cumbersome process to feed the antenna efficiently,

which consequently affects the accuracy of measurement results for gain and bandwidth [17].

2.4 Miniaturization Techniques

Different miniaturization techniques have been developed over the years to alleviate the aforementioned shortcomings and improve radiation efficiency of the antenna. Techniques used in mobile communications include using high-contrast dielectric materials, shorting vias, incorporated lumped elements within antenna structures, and slotted patch to influence the radiation of the antenna [18-22]. Some of these techniques will be briefly reviewed in the following sections.

2.4.1 Lumped-Element Loaded Antennas

This method is a relatively straightforward method of making antenna smaller in size compared to other methods without disrupting any resonant features. It is usually applied to antennas that are smaller than half a wavelength in order to neutralize the strong reactive impedance. A major drawback of the lumped element method is the limited bandwidth, as reported in [18], wherein a novel idea was proposed to use distributed lumped elements within the antenna geometry to modify the input impedance of the antenna and thus miniaturize its size over a broad frequency range. A resonant transmission line loop antenna with a 43% miniaturization was developed without altering its original field behavior.

2.4.2 Antennas Loaded With Materials

The resonating frequency of a circular microstrip patch antenna depends on the dielectric permittivity based on equation (2.4). Therefore, loading the patch antenna with a high-contrast dielectric material reduces its resonant frequency. Microstrip patch antennas with thick substrate and dielectric constant of 10 to 13 were examined in [19] for miniaturization purposes. Their radiation performances were found different from those of conventional antennas. It was observed that the measured input impedances were lower than their theoretical values for thin substrates. In [20], ceramic substrates with the dielectric constant of 58 were used to reduce the size of a square ring microstrip patch antenna. Circular polarization was achieved by a simple microstrip feed line through the aperture coupling method operating at 1.573 GHz. The new size of the microstrip patch antenna with the dielectric loading was 50% smaller than the conventional antenna.

In addition to ceramic substrates, magneto-dielectric substrate was also used for the miniaturization of microstrip patch antennas [21]. Compared to the reference antenna, the area of the magneto-dielectric-loaded antenna was reduced by 65% at 2.45 GHz. High permittivity dielectric materials reduce the antenna directivity, which may be useful in wide angular coverage applications. The material loading technique, however, increases the mass of the antenna unit and also makes it expensive [22]. By using high-contrast dielectric constant materials, the surface wave propagation will increase within the substrate, lowering the radiation efficiency and the bandwidth due to the increased losses.

2.4.3 Antenna Loaded With Shorting Vias

Another cost-effective approach to miniaturize an antenna is to use shorting posts or metallic vias, which connect the ground plane to the radiating patch. This method reduces the resonating frequency and thus shrinks the dimensions of the antenna patch. This methodology of reducing the antenna size was first used by Waterhouse [23]. In [24], it was shown that the resonant frequency depends critically on the position and the dimensions of the shorting posts. These observations were largely made on a phenomenological basis, i.e., on experimental or simulation results. A circular microstrip patch loaded with shorting vias was presented in [24], which provided conical beams identical to higher mode antennas. Based on the parametric analysis, it was stated that decreasing the radius of the vias reduced the resonance frequency. Narrower vias provided further miniaturization of the microstrip patch. A parametric analysis was conducted to examine the effects of numbers of vias, from which it was concluded that the miniaturization factor of the antenna could potentially improve with more shorting vias. However, the antenna gain would be compromised.

2.4.4 Meandering Method

This technique is based on the conception of lowering resonant frequency by increasing the effective electrical path of the surface currents using slots or slits to meander the current path. Representative meandered currents in a rectangular patch are illustrated in Fig. 2.3, where the current path is elongated by the insertion of several slits within the patch, which consequently reduce the resonance frequency.

(a)   (b)
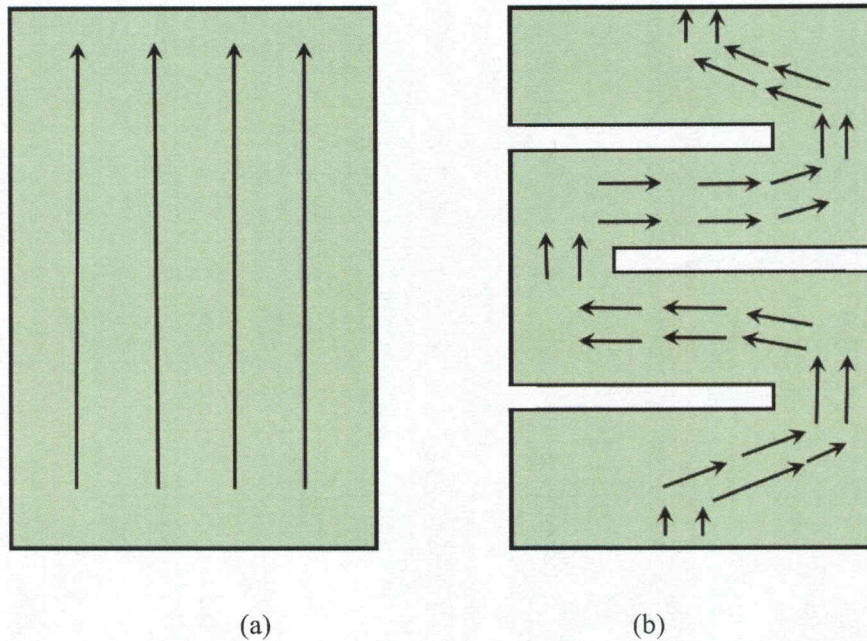
Fig. 2.3: Surface current distributions for (a) ideal rectangular patch (b) rectangular patch loaded with slits.

The slit loading technique is also used to generate desired polarization. A circular polarization can be generated by placing slits symmetrically to the center. The miniaturization ratio depends on the dimensions and position of the slits on the radiating patch. R. Pascaud et al. [22] designed a slit-loaded antenna at 161 MHz for satellite applications. Multiple slits were incorporated on the ring shaped patch structure to reduce the resonant frequency. A parametric analysis was undertaken to finalize the length and the number of slits. The authors achieved a maximum reduction in resonant frequency by a factor of 1.73 with a good impedance matching of below -20 dB. Meandering the current path to miniaturize antenna is a robust and inexpensive method, however it may have a detrimental impact on the polarization purity of the antenna.

2.5 Summary

In this chapter, circular microstrip patch antennas made of perfect electric conductor were analyzed and the governing equations based on the cavity model were reviewed for higher order modes. The benefit of operating the patch at a higher mode is that it provides a null at the boresight direction, subsequently reducing the impact of interference on the signals. A major drawback of using higher order mode antennas is their enlarged aperture areas. With advancements in the miniaturization of communication systems, many techniques have been developed to decrease the size of the antenna structure, which also adversely impacts it radiation efficiency, gain, bandwidth, and other characteristics. Based on the required miniaturization factor, proper techniques, some of which were reviewed in this chapter, can be employed to reduce the antenna size. In this thesis, the slit loading method will be utilized in order to decrease the radius of circular microstrip patch antennas excited at higher order modes close to that at the dominant mode.

CHAPTER 3

A Miniaturized TM_{21} Mode Circular Microstrip Patch Antenna

3.1 Introduction

Microstrip patch antennas (MPAs) have become an appropriate candidate for portable antenna systems, due to their compact and low-profile configurations. A microstrip patch antenna, backed by a thin grounded dielectric slab, mainly supports transverse magnetic (TM) modes, as discussed in Chapter 2. Certain higher order TM_{nm} modes produce conical radiation patterns with a null at the boresight direction, providing numerous advantages in satellite communications, wireless local area network (LAN), tracking and guiding systems, and anti-jamming applications, where the null can be directed towards the source of the interference. However, the main issue with these higher order modes is that they require much larger aperture size compared with the dominant TM_{11} mode, whose radius is $0.293\lambda_d$ [7], where λ_d is the guided wavelength. For the mode of interest in this chapter, i.e. the TM_{21} mode, the radius of the patch should be enlarged to $0.486\lambda_d$ [7], which has hindered its applications in tightly-spaced antenna and array configurations. Thus, this chapter focuses on miniaturizing a circular microstrip patch antenna operating at the TM_{21} mode, such that its radius is reduced to that of the TM_{11} modes, i.e. $0.293\lambda_d$. The proposed method is based on a judicial alteration in the patch geometry, which is inspired by the surface current distributions of the TM_{21} mode. As such, a cost-effective miniaturization technique is developed without adding any extra mass to the antenna unit.

3.2 Conventional TM$_{21}$ Mode Circular Patch Antennas

Based on the cavity model discussed in Chapter 2, the radius of a circular patch is governed by Equation (2.4), using the eigenvalues of each mode, as listed in Table 2.1. These eigenvalues are determined by applying the magnetic wall boundary condition. That is, at the periphery of the radiating patch the magnetic field should vanish. For the TM$_{21}$ mode under investigation, the corresponding eigenvalue, i.e. χ_{21}, is 3.05424, and thus the radius of the patch is given by [7],

$$a_{21} = \frac{3.05424 \, \lambda_o}{2\pi\sqrt{\varepsilon_{eff}}} = 0.486 \, \lambda_d \qquad (3.1)$$

where ε_{eff} is the effective dielectric constant due to the fringing electric fields, λ_o is the free-space wavelength, and λ_d is the dielectric wavelength expressed by,

$$\lambda_d = \frac{C}{f\sqrt{\varepsilon_{eff}}} \qquad (3.2)$$

where C is the speed of light in free space and f is the operating frequency of the antenna, which is 5 GHz for the conventional TM$_{21}$ mode patch antenna. As presented in Chapter 2 using the cavity model assuming an infinite ground plane, the spherical components of the radiated electric fields are given by the following equations for a circular patch antenna, of radius a_{21}, operating at the TM$_{21}$ mode at the far-field region [7].

$$E_\theta = -\frac{V a_{21} \kappa_o}{4} \frac{e^{-j\kappa_o r}}{r} \left(J_3(\kappa a_{21} \sin(\theta)) - J_1(\kappa a_{21} \sin(\theta)) \right) \cos 2\phi \qquad (3.3)$$

$$E_\phi = -\frac{V a_{21} \kappa_o\, e^{-j\kappa_o r}}{4} \frac{e^{-j\kappa_o r}}{r} \cos\theta\, (J_3(\kappa a_{21} \sin(\theta)) + J_1(\kappa a_{21} \sin(\theta)))\, \sin 2\phi \tag{3.4}$$

Typical far-field radiation patterns for the TM_{21} mode are plotted in Fig. 3.1. As expected, the main beam is split and the antenna generates a conical radiation pattern with a null at the boresight direction of $\theta = 0°$. Due to the infinite ground plane size, the back radiation is zero.
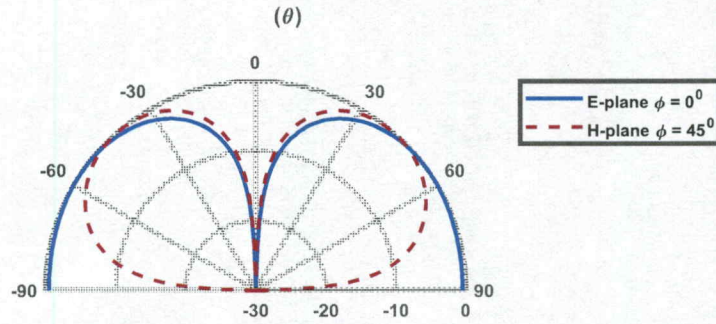
Fig. 3.1: Typical far-field radiation patterns of a TM_{21} mode circular patch antenna with $a_{21}=0.486\lambda_d$, backed by an infinite ground plane.

For a reference case, a conventional microstrip patch antenna at the TM_{21} mode, whose geometry is depicted in Fig. 3.2, is designed to resonate at 5 GHz. For practical applications, a truncated ground plane size that is sufficiently large to reduce the back radiation needs to be used. As such, the reference TM_{21} patch is mounted on a circularly shaped grounded dielectric slab with a radius of 60 mm, which is equal to one wavelength at 5 GHz. The radius of the patch, denoted by a_{21} in Fig. 3.3, is 19.25 mm. The antenna is fed by a 50-Ω coaxial probe with a feed point offset 10 mm from the center of the circular patch. The substrate is RT Duroid 5880 [25] with $\varepsilon_r=2.2$ and a thickness of 1.6 mm. The

21

design specifications of the reference TM$_{21}$ mode circular patch antenna is listed in Table 3.1.

Table 3.1: Design specifications of a circular microstrip patch antenna operating at TM$_{21}$ mode.

Design Parameters	Design values
Frequency	5 GHz
Height of the substrate (h)	1.6 mm
ε_r	2.2
Loss Tangent	0.0009
Substrate Material	RT Duroid 5880
Radius of the patch (a_{21})	19.25 mm
Radius of the ground (R_g)	60 mm
Probe feed from the center (ρ)	10 mm

(a)   (b)
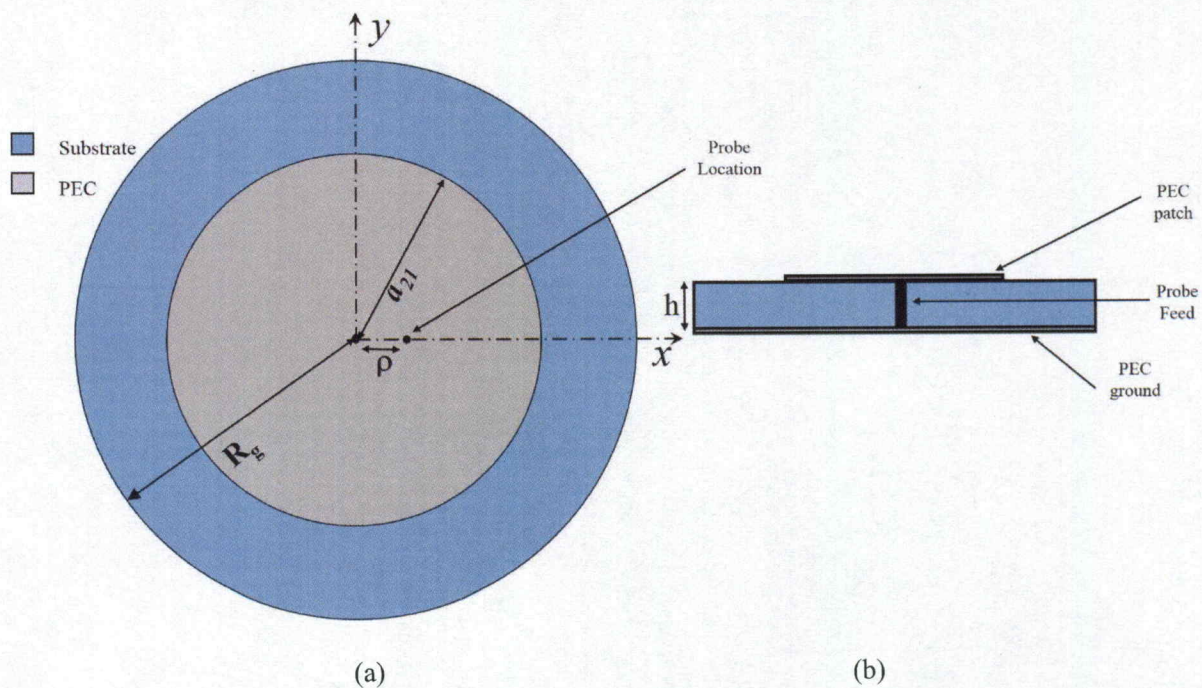
Fig. 3.2: (a) Top- and (b) side-view of a conventional TM$_{21}$ mode circular patch antenna at 5 GHz with a_{21} = 19.25 mm, Rg = 60 mm, ρ = 10 mm, and h = 1.6 mm.

3.3 Proposed Miniaturized TM$_{21}$ Circular Microstrip Patch Antenna

As per Equation (3.1), if a conventional TM$_{21}$ mode is to be used in an array configuration, a minimum element spacing of $0.972\lambda_d$ would be required, which would cause grating lobes. Therefore, there is a need to reduce the size of the patch at this specific mode. The proposed method [26] in this thesis is based on a geometrical alteration in the patch layer, leading to an inexpensive miniaturization method. The technique is inspired by the surface current distributions of the patch antenna at its TM$_{21}$ mode, illustrated in Fig. 3.3. As it is observed, there are four distinct peak intensities of the surface current distributions in each of the four quadrants of the disk. Therefore, if one places a radial slit in each of these quadrants, the current path will be meandered, which eventually miniaturizes the antenna size.
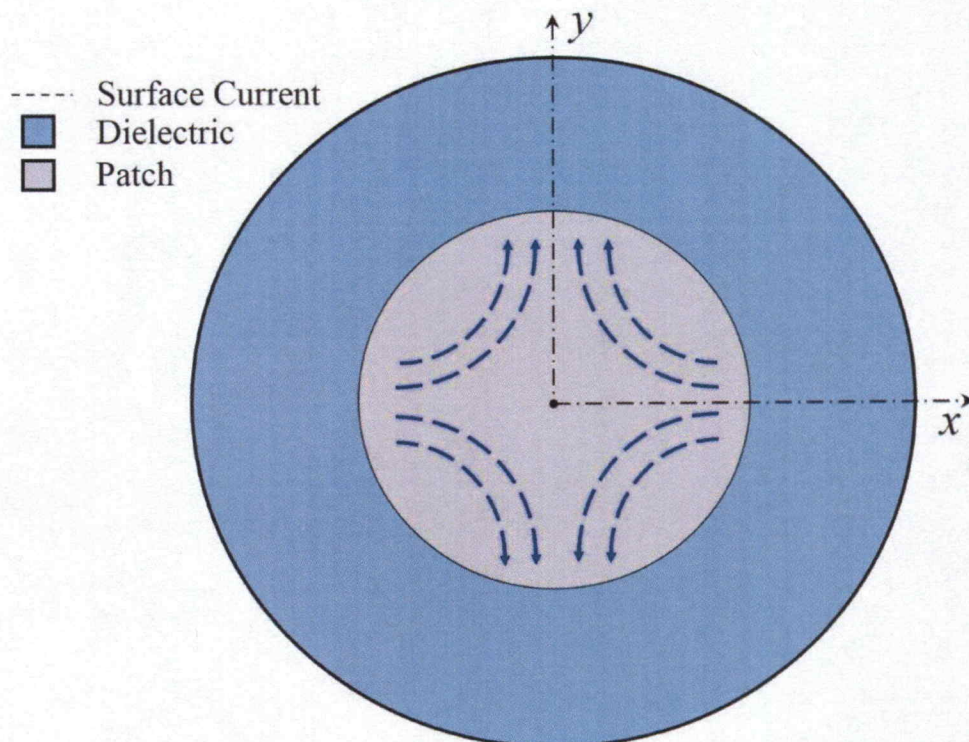
Fig. 3.3: Typical surface current distribution of a circular patch antenna operating at the TM$_{21}$ mode.

The proposed antenna [26] is depicted in Fig. 3.4, where four slits are radially cut from the patch in each quadrant. The slits are curved trapezoids to intercept most of the current path and are symmetrically arranged with a 90° angular spacing. The slit is defined by its length and angular opening, denoted by L and α, respectively, as shown in Fig. 3.4. These two parameters play a key role in miniaturizing the TM_{21} patch size.
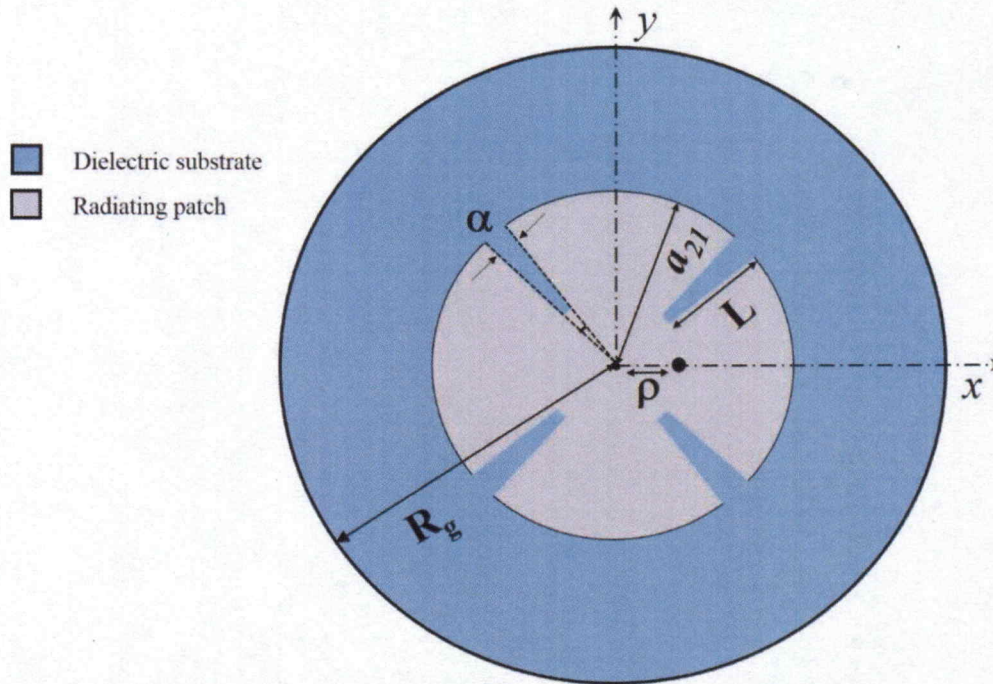
Fig. 3.4: Geometry of the proposed slit-loaded TM_{21} circular patch antenna with $a_{21} = 19.25$ mm; Rg = 60 mm, ρ= 4.2 mm, ε_r = 2.2, and h = 1.6 mm.

Similar to the reference antenna, the radius of the patch, denoted by a_{21} in Fig. 3.4, is 19.25 mm, and the ground and substrate have a diameter of 120 mm. Due to the presence of the slits, a slight adjustment needs to be made in the probe location to improve the impedance matching. That is, the 50-Ω coaxial probe is now offset 4.2 mm from the center of the circular patch. When L=13 mm and α=4.2°, the resonant frequency of the TM_{21} mode will reduce to about 3 GHz, which is equal to the resonant frequency of the dominant TM_{11} mode, implying that one may excite the TM_{21} mode within the same aperture area required

for the conventional dominant-mode patch antennas. The values of L and α were concluded based on the parametric study, as will be detailed in the following sections.

3.4 Effect of the Slits on Antenna Miniaturization

An extensive parametric study has been conducted to finalize the design, resulting in about 40% reduction in the radius of the radiating patch. In the following sections, the effect of the slit length and slit opening on the resonance frequency of the antenna will be investigated.

3.4.1 Varying Slit Length

In this section, the impact of the slit length, denoted by L in Fig. 3.4, on the resonance frequency is investigated by analyzing the proposed antenna with the finite-element based full-wave electromagnetic solver ANSYS HFSS v.18 [27]. The reflection coefficients are plotted in Fig. 3.5, where L changes from 0 mm to 13 mm for a fixed α of 4.2°. As can be seen, the resonant frequencies of the TM_{11} and TM_{21} modes of the unloaded patch, i.e. the $L=0$ case, occur at 3 GHz and 5 GHz, respectively. By placing four symmetrical slits in each of the quadrants of the patch, the resonant frequency of the TM_{21} mode starts decreasing as the slits force the current to meander, helping in increasing the electric size of the patch. Consequently, the resonance frequency decreases as the slit length increases. In particular, the frequency reaches to that of the TM_{11} mode, when the slit length is 13mm. As for the dominant mode, its resonant frequency is slightly impacted by the slits. That is, it shifts down from 3 GHz to 2.3 GHz when $L=0$ and $L=13$mm, respectively. This allows one to design a TM_{21} mode circular patch antenna with the same aperture size as

the conventional dominant mode. The reflection coefficient is reasonably in the acceptable

limit of below -10 dB level for different slit lengths for the TM$_{21}$ mode.
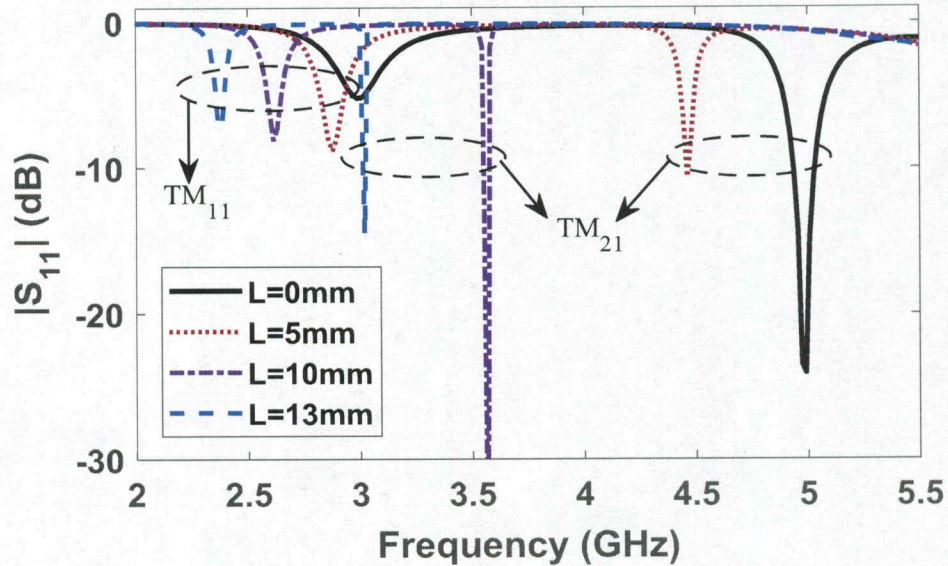
Fig. 3.5: Reflection coefficients of the proposed antenna in Fig. 3.4 for different slit lengths with α=4.2°.

For the TM$_{21}$ mode, a summary of the resonant frequencies, gain, and size reduction

of the conventional and miniaturized TM$_{21}$ patch antennas is listed in Table 3.2 for different

slit lengths. The resonant frequency of the TM$_{21}$ mode reduces from 5 GHz to 3 GHz,

resulting in about 40% and 64% reductions in its radius and area, respectively. Similar to

other miniaturized antennas, the gain is compromised, as expected. That is, the peak gain

drops by about 4.5 dB and 1.35 dB at the E- and H-planes, respectively.

Table 3.2: Impact of varying L on resonant frequency, S_{11}, and gain of the slit-loaded patch antenna shown in Fig. 3.4, when $\alpha = 4.2°$.

L (mm)	Frequency (GHz)	S_{11} (dB)	Gain (dBi)		% reduction of radius	% reduction of area
			$\phi = 0°$	$\phi = 45°$		
0	5	-25.38	7.25	3.75	N/A	N/A
5	4.44	-10.04	5.37	5.28	11.2%	21.23%
10	3.57	-31.02	4.42	4.34	28.6%	49.3%
13	3.0126	-17.8	2.63	2.39	**39.7%**	**64%**

3.4.2 Varying Slit Opening

As depicted in Fig. 3.4, each slit has an angular opening, which is defined by α. The effect of α on the resonance frequency is investigated in this section. The reflection coefficients are shown in Fig. 3.6, when the opening angles vary from 0 to 4.2° for a fixed length of $L = 13$mm.
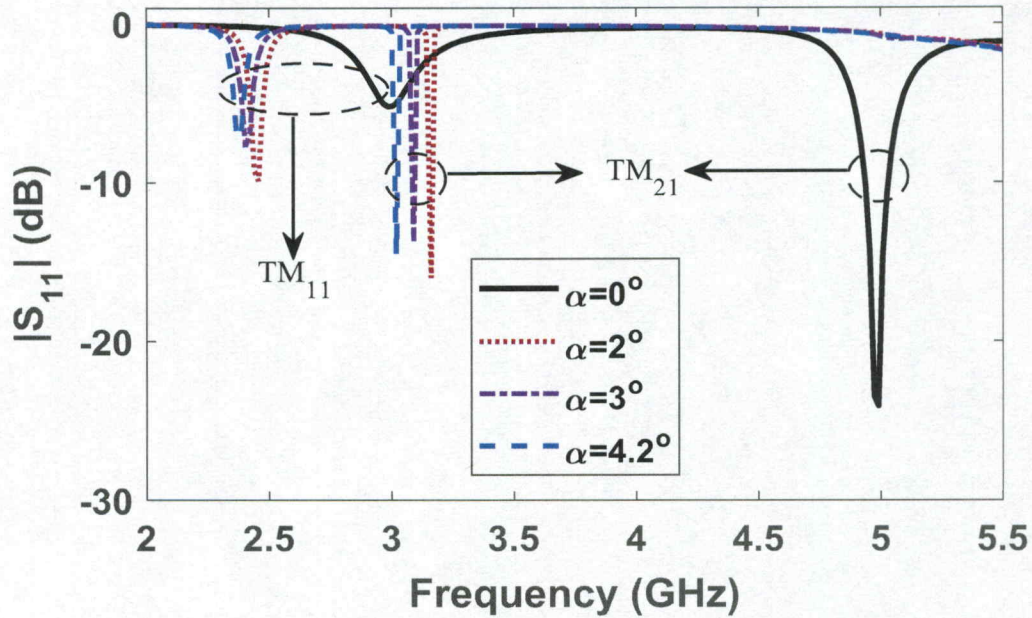
Fig. 3.6: Reflection coefficients of the proposed antenna in Fig. 3.4 for different slit angles with L=13mm.

The opening angle (α) provides another degree of freedom to further control the miniaturization such that it finely tunes the resonant frequency of the TM_{21} mode to 3 GHz,

which results in an eigenvalue of 1.841 for the miniaturized TM_{21} mode. As it is shown in Fig. 3.6, the resonant frequency of the TM_{21} mode decreases as α increases. The decrease in resonant frequency due to the change in α is not as significant as varying the length of the slot. The slight shift in resonance frequency is also seen on the dominant mode of the antenna. A summary of the resonant frequencies, gain, and size reduction of the conventional and miniaturized TM_{21} patch antennas is provided in Table 3.3 for different slit angles.

Table 3.3: Impact of varying α on resonant frequency, S_{11}, and gain of the slit-loaded patch antenna shown in Fig. 3.4, when $L = 13$ mm.

α°	Frequency (GHz)	S_{11} (dB)	Gain (dBi)		% reduction of radius	% reduction of area
			$\phi = 0^\circ$	$\phi = 45^\circ$		
0°	5	-25.38	7.25	3.75	-	-
2°	3.17	-19.5	2.88	2.87	36.6%	56.7%
3°	3.10	-15.92	2.65	2.80	38%	61%
4.2°	3.0126	-17.8	2.63	2.39	**39.7%**	**64%**

3.5 Comparison of Conventional and Miniaturized TM_{21} Patch Antennas

3.5.1 Full-Wave Numerical Results

As presented in Section 3.4, the proposed antenna with the finalized slit size of $L = 13$mm and $\alpha = 4.2^\circ$ results in about 40% reduction in the patch radius. Thus, it is instructive to further investigate how the antenna performs after miniaturization by comparing its characteristics, including radiation patterns and surface current intensities, with a conventional TM_{21} patch antenna. In this section, the numerical results of such comparisons are provided.

Fig. 3.7 compares the reflection coefficients of the conventional antenna and the proposed antenna. The resonance frequency of the TM_{21} mode in the slit loaded patch has reduced by almost 40%, equivalent to a 64% reduction in the patch area, which is quite significant. The geometrical alteration of the radiating patch has reduced the frequency of the dominant mode by 23.3%. These results are also summarized in Table 3.4 for both dominant TM_{11} and the higher TM_{21} modes.

Table 3.4: Reduction in frequency for different modes unloaded case and slit loaded case for TM_{21} circular patch antenna

Mode	TM_{11}		TM_{21}	
	Before Miniaturization	After Miniaturization	Before Miniaturization	After Miniaturization
Frequency (GHz)	3	2.36	5	3
Radius	$0.293\lambda_o$	$0.230\lambda_o$	$0.486\lambda_o$	$0.293\lambda_o$
χ	1.841	1.445	3.054	1.841
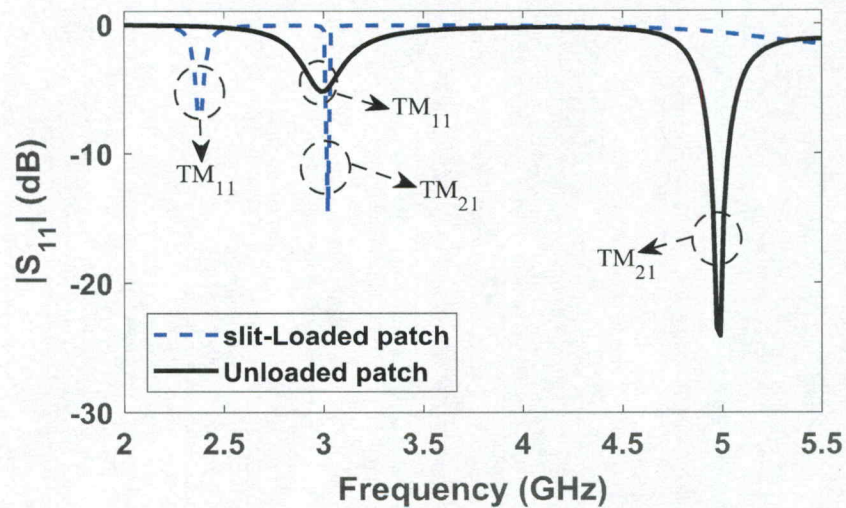
Fig. 3.7: Reflection coefficients of the unloaded patch and slit-loaded patch antenna in Fig. 3.4 with $L = 13$ mm and $\alpha = 4.2°$

Radiation patterns of the conventional antenna and the proposed miniaturized antenna are also compared at both TM_{11} and TM_{21} modes. Fig. 3.8 shows radiation patterns before and after miniaturization for the dominant TM_{11} mode at their respective resonant frequencies of 3 GHz and 2.36 GHz. They both have broadside radiation patterns with the peak at the $\theta=0^\circ$ direction, as expected. Due to the smaller miniaturization factor for this mode, the peak gain only drops by 1.2 dBi. To shed light on this, the corresponding surface current distributions of the TM_{11} mode are illustrated in Fig. 3.9, before and after miniaturization at the aforementioned resonant frequencies. The peak gain at this mode is affected insignificantly. This is because only a small fraction of the current path, which is almost vertically aligned, is impacted by the four diagonal slits.

Unlike the dominant mode, the gain drop is expected to be significant for the TM_{21} mode as the slits are placed to influence TM_{21} mode, whose radiation patterns are plotted in Fig. 3.10 before and after miniaturization at their respective resonant frequencies of 5 GHz and 3 GHz. More specifically, the peak gain now drops by about 4.5 dB and 1.35 dB at the E- and H-planes, respectively. This is mainly attributed to the fact that the effective aperture area of the antenna becomes smaller after miniaturization. As such, the gain is compromised, based on the aperture theory [2]. For further clarification, the associated surface current distributions are depicted in Fig. 3.11 for the TM_{21} mode before and after miniaturization. For the latter, the meandered current path is clearly visible around the radial slits, which subsequently decreasing the resonant frequency of the TM_{21} mode circular patch antenna. The novelty of the proposed design is that one may use the same eigenvalue of the conventional TM_{11} mode, equal to 1.841, to design such a miniaturized TM_{21} patch antenna.
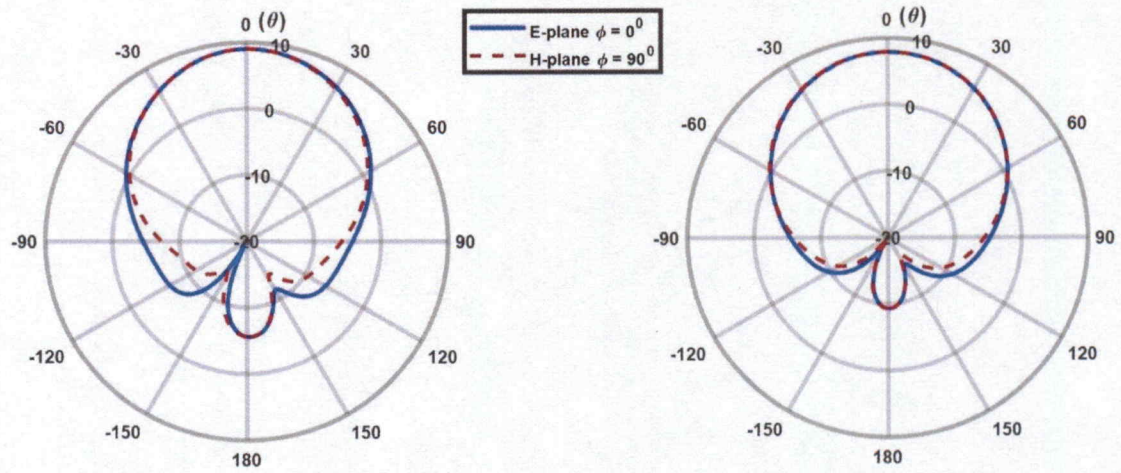
(a)   (b)

Fig. 3.8: Radiation patterns of the TM_{11} mode for (a) the unloaded patch of $L=0$ and at 3 GHz (b) the proposed antenna in Fig. 3.4 of $L = 13$ mm and $\alpha = 4.2°$ at 2.36 GHz.
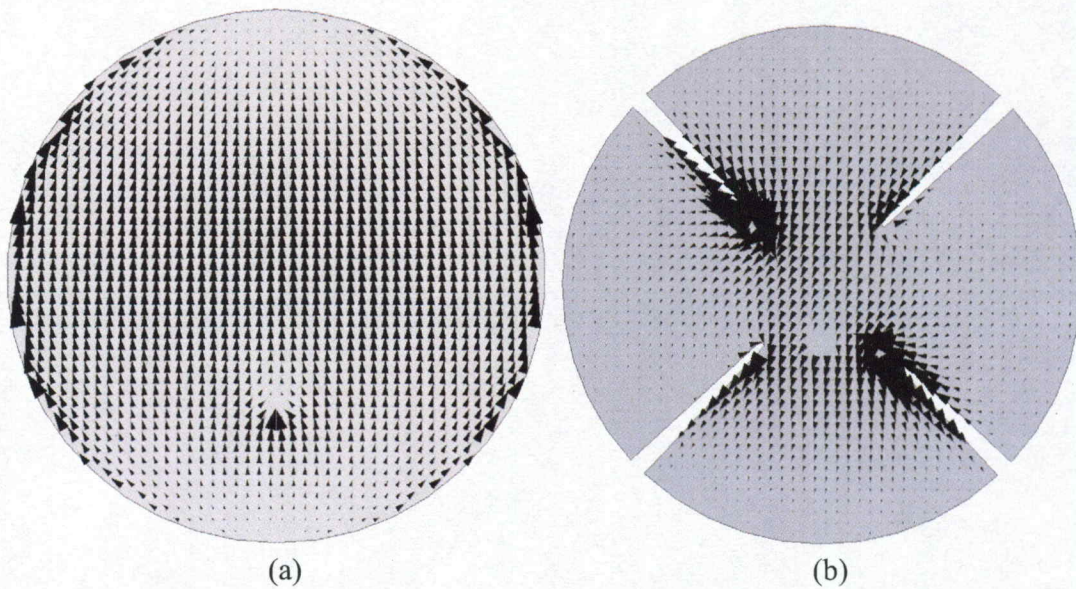
(a)   (b)

Fig. 3.9: Surface current distributions of the TM_{11} mode for (a) the unloaded patch of $L=0$ and at 3 GHz (b) the proposed antenna in Fig. 3.4 of $L=13$mm and $\alpha = 4.2°$ at 2.36 GHz.
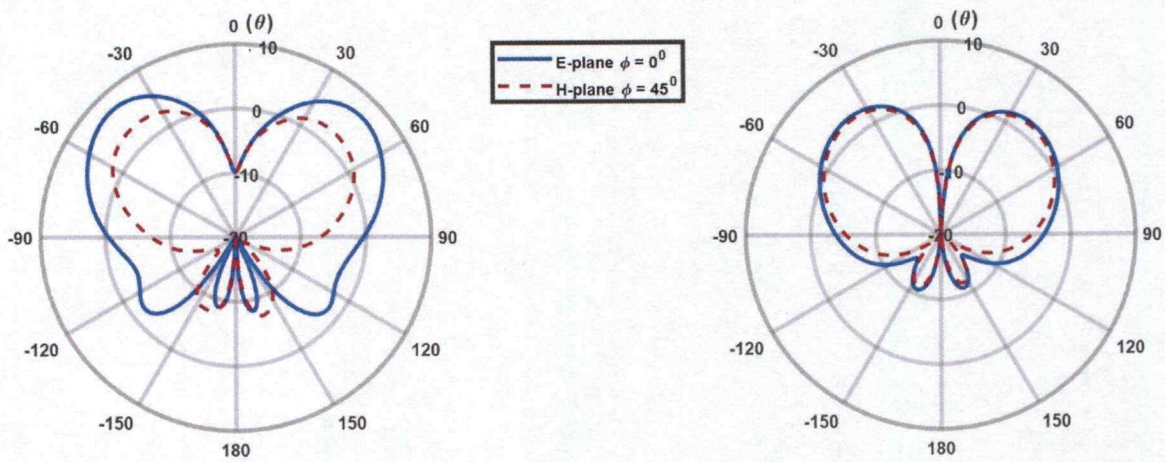
(a)   (b)

Fig. 3.10: Radiation patterns of the TM_{21} mode for (a) the unloaded patch of $L=0$ and at 5 GHz (b) the proposed antenna in Fig. 3.4 of $L=13$mm and $\alpha = 4.2°$ at 3 GHz.
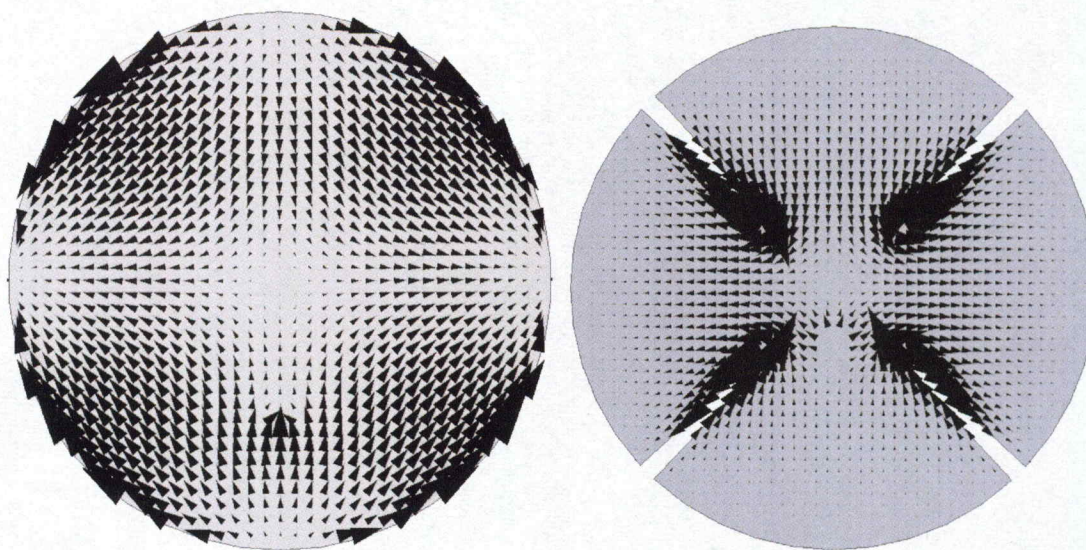
(a)   (b)

Fig. 3.11: Surface current distributions of the TM_{21} mode for (a) the unloaded patch of $L=0$ and at 5 GHz (b) the proposed antenna in Fig. 3.4 of $L=13$mm and $\alpha = 4.2°$ at 3 GHz.

32

The three-dimensional radiation pattern of the finalized miniaturized patch antenna with L=13mm and α = 4.2° is shown in Fig. 3.12 for the TM$_{21}$ mode at the frequency of 3 GHz. The main beam is split and the pattern has a null at the boresight angle of θ=0°, as expected.
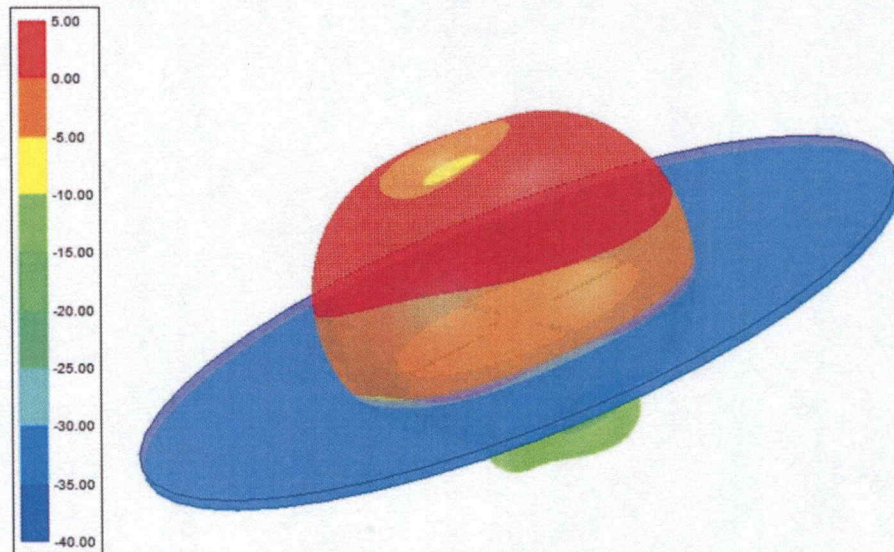
Fig. 3.12: The three-dimensional radiation pattern of the miniaturized TM$_{21}$ circular patch in Fig. 3.4 of L=13mm and α = 4.2° at 3 GHz.

3.5.2 Measurement Results

To validate the full-wave numerical results shown in preceding sections, the proposed miniaturized circular patch antenna loaded with four identical slits of L = 13 mm and α=4.2° was fabricated using the printed circuit board (PCB) technology. In this section, the simulation and measurement results of reflection coefficients and radiation patterns will be compared and discussed.

Fig. 3.13 (a) shows the top view of the fabricated antenna. A photograph of the antenna under test inside the spherical near-field anechoic chamber of the University of Alabama in Huntsville is also shown in Fig 3.13 (b).

Fig. 3.14 compares the resonant frequencies of simulated and measured results of the proposed slit loaded antenna, which are in good agreement. As can be seen, the frequency of the miniaturized TM_{21} mode is reduced to that of the dominant mode with no slits. This confirms that the eigenvalue and the size of the patch have been reduced accordingly.

(a)

(b)
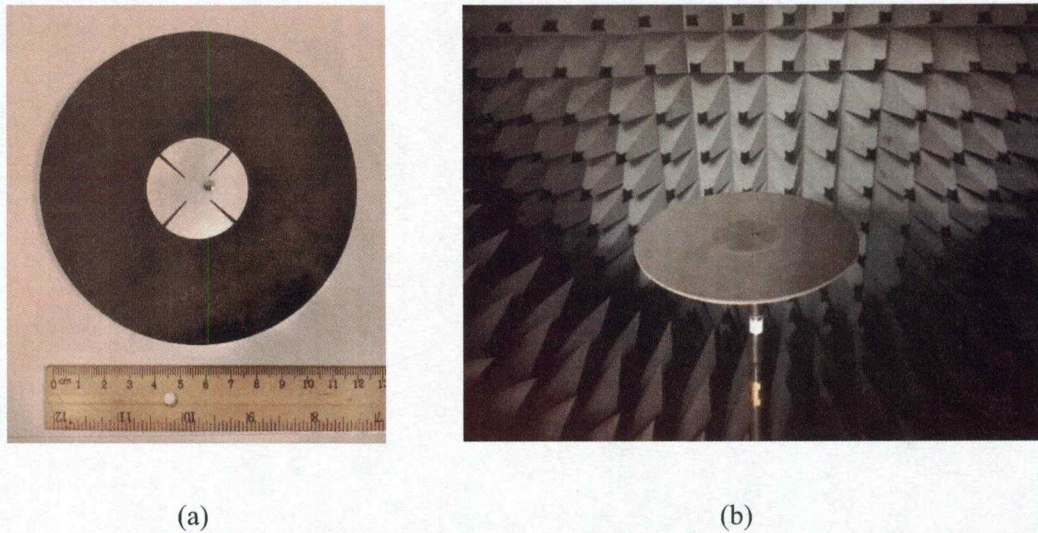
Fig. 3.13: (a) Top view of the fabricated miniaturized circular patch antenna and (b) a photo of the antenna under test with L = 13 mm and α = 4.2°.
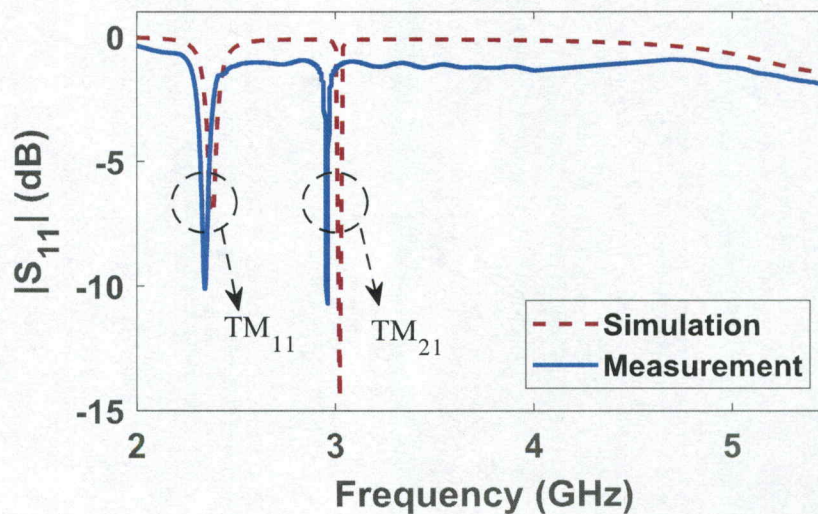
Fig. 3.14: Simulated and measured reflection coefficients of the fabricated antenna, with L = 13 mm and α = 4.2°.

The radiation patterns of the prototype antenna were measured at 3 GHz in the spherical near-field anechoic chamber. The results are plotted in Fig. 3.15 and compared with the simulated results at the E- and H-planes. Overall, the results are in good agreement, except there is a slight difference in the right-hand side of the pattern, which is mainly due to the reflections from the connecting cable to the antenna, contributing to the asymmetry observed in the patterns. Nonetheless, a conical radiation pattern is obtained with a null at the boresight direction of $\theta=0°$. The null at the center of the radiation pattern and the overall profile of the pattern confirm that the antenna operates at the TM_{21} mode.

(a)   (b)
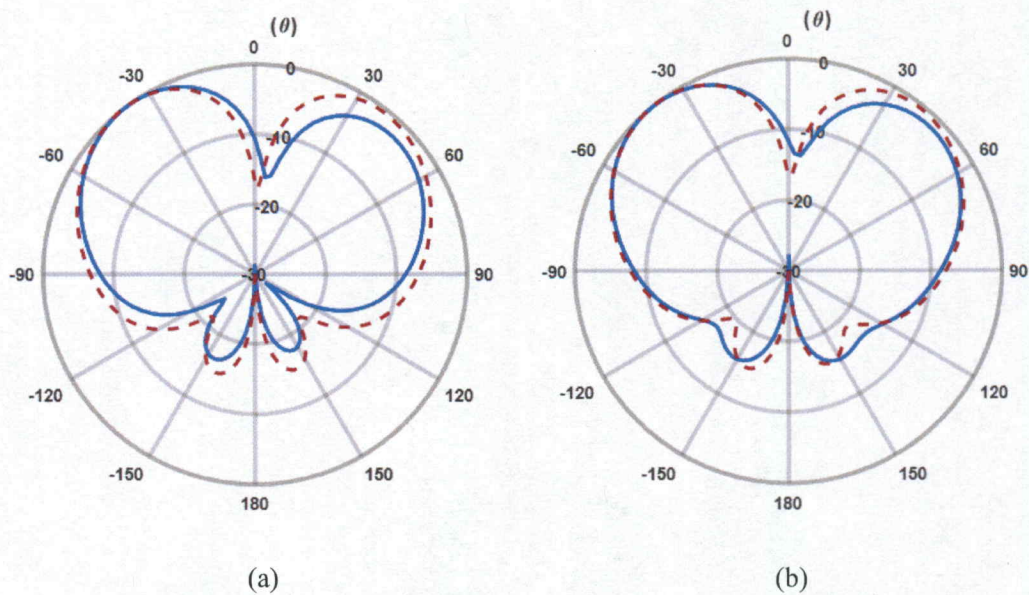
Fig. 3.15: Measured and simulated normalized radiation patterns of the fabricated antenna in Fig. 3.13 at 3 GHz, when $L = 13$ mm and $\alpha = 4.2°$. (a) E-plane at the $\phi = 0°$ plane (b) H-plane at the $\phi = 45°$ plane; —— Measured ---- simulated.

3.6 Summary

A novel miniaturized circular patch antenna operating at the TM_{21} mode was introduced. The miniaturization was realized by placing four radial slits to elongate the

current path and thus reduce the aperture size of the antenna. A parametric study was conducted to understand the effects of the slits on the size reduction, gain, and reflection coefficients. It was concluded that size of the patch can be controlled by changing the radial and angular dimensions of the slits. Reduction up to 40% and 64% has been achieved in the patch radius and area, respectively, which makes its aperture size equal to that of the conventional dominant mode.

CHAPTER 4

A Miniaturized TM$_{31}$ Mode Circular Patch Antenna

4.1 Introduction

Microstrip patch antennas have been widely used in satellite communications and anti-jamming applications as mentioned in previous chapters. Microstrip patch antennas when excited at the dominant mode will have a broadside radiation pattern, resulting in a low resolution at low elevation angles [3]. Although the planar arrays of these elements provide high gain at the boresight region, the radiation intensity reduces towards lower elevation angles. This is undesirable for low-elevation satellites. Hence, antennas with conical radiation patterns are needed, which facilitate effective communications with satellites and transmitters at low elevation angles. Among planar antennas, circular microstrip patches operating at the TM$_{n1}$ modes are excellent candidates for such applications, as their main beams move towards the horizon as the mode index number n increases. The TM$_{31}$ mode is studied in this Chapter for miniaturization.

To excite the TM$_{31}$ mode in a circular patch, the radius of the patch should be enlarged to $0.668\lambda_d$ [7], which imposes even more spatial limitation than the TM$_{21}$ mode in compact antenna and array units. Therefore, similar to Chapter 3, the main objective is to miniaturize the TM$_{31}$ mode circular patch such that its radius becomes close to that of the dominant mode, i.e. close to $0.293\lambda_d$. Inspired by its surface current distributions, the slit-loading technique will be judiciously utilized to realize a cost-effective size reduction without adding any extra mass to the antenna structure.

4.2 Conventional TM$_{31}$ Mode Circular Patch Antennas

The radius of the patch operating at the TM$_{31}$ mode is determined based on the cavity model discussed in Chapter 2 and is governed by Equation (2.4). For the TM$_{31}$ mode, the associated eigenvalue χ_{31} is 4.20119, as listed in Table 2.1. Thus, the radius of the patch operating at the TM$_{31}$ mode is given by [7].

$$a_{31} = \frac{4.20119\,\lambda_o}{2\pi\sqrt{\varepsilon_{eff}}} = 0.668\,\lambda_d \tag{4.1}$$

where ε_{eff} is the effective dielectric constant due to the fringing electric fields and λ_d is the dielectric wavelength, expressed by,

$$\lambda_d = \frac{C}{f\sqrt{\varepsilon_{eff}}} \tag{4.2}$$

where C is the speed of light in free space and f is the operating frequency of the antenna, which is 5 GHz for the conventional TM$_{31}$ mode patch antenna. As presented in Chapter 2 using the cavity model assuming an infinite ground plane, the spherical components of the radiated electric fields are given by the following equations for a circular patch antenna of radius a_{31}, operating at the TM$_{31}$ mode at the far-field region [7].

$$E_\theta = -j\frac{Va_{31}\kappa_o}{4}\frac{e^{-j\kappa_o r}}{r}\left(J_4(\kappa a_{31}\sin(\theta)) - J_2(\kappa a_{31}\sin(\theta))\right)\cos 3\phi \tag{4.3}$$

$$E_\phi = -j\frac{Va_{31}\kappa_o}{4}\frac{e^{-j\kappa_o r}}{r}\cos\theta\left(J_4(\kappa a_{31}\sin(\theta)) + J_2(\kappa a_{31}\sin(\theta))\right)\sin 3\phi \tag{4.4}$$

Typical far-field radiation patterns of the TM_{31} mode are depicted in Fig. 4.1. As expected, the main beam is split and the antenna generates a conical radiation pattern with a null at the boresight direction of $\theta = 0^\circ$, now having the main lobe at much lower elevation angle θ compared with the TM_{21} mode. Due to the infinite ground plane size, the back radiation is zero.
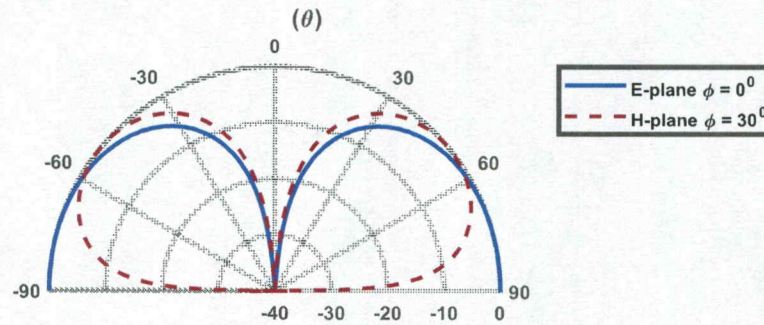
Fig. 4.1: Typical far-field radiation patterns of a TM_{31} mode circular patch antenna with $a_{31}=0.668\lambda_d$, backed by an infinite ground plane.

Geometry of a conventional microstrip patch antenna operating at the TM_{31} mode is illustrated in Fig. 4.2, which is to resonate at 5 GHz. To reduce the back lobe in the radiation pattern a truncated ground plane needs to be used, which should be sufficiently large to avoid any edge diffractions. As such, the reference TM_{31} patch is mounted on a circularly shaped grounded dielectric slab with a radius of 60 mm, which is equal to one wavelength at 5 GHz. The radius of the patch, denoted by a_{31} in Fig. 4.2, is 26.75 mm. The antenna is fed by a 50-Ω coaxial probe with a feed point offset 17 mm from the center of the circular patch. The substrate is RT Duroid 5880 [25] with ε_r=2.2 and a thickness of 1.6 mm. The design specifications of the reference TM_{31} mode circular patch antenna are listed in Table 4.1.

Table 4.1: Design specification of a circular microstrip patch antenna operating at the TM_{31} mode.

Design Parameters	Design values
Frequency (f)	5 GHz
Height of the substrate (h)	1.6 mm
ε_r	2.2
Loss Tangent	0.0009
Substrate Material	RT Duroid 5880
Radius of the patch (a_{31})	26.75 mm
Radius of the ground (R_g)	60 mm
Probe feed from the center (ρ)	17 mm

(a)   (b)
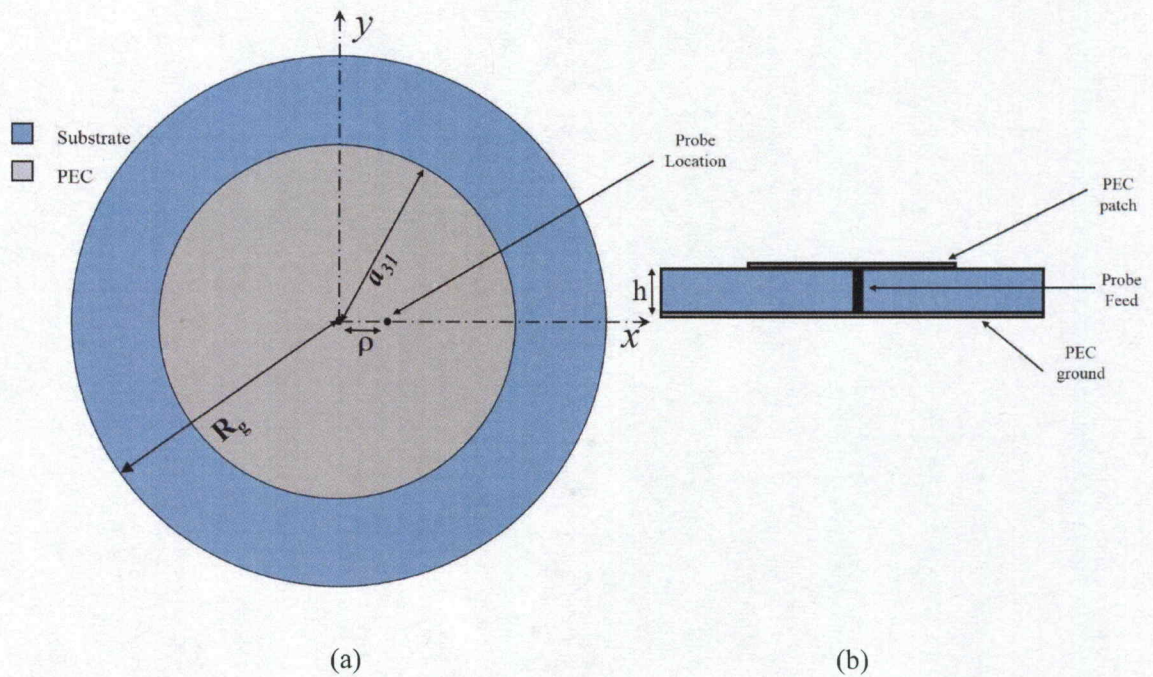
Fig. 4.2: (a) Top- and (b) side-view of a conventional TM_{31} mode circular patch antenna at 5 GHz with a_{31} = 26.75 mm, R_g = 60 mm, ρ = 17 mm, ε_r = 2.2, and h = 1.6 mm.

4.3 Proposed TM$_{31}$ Circular Microstrip Patch Antenna

As detailed in Section 4.2, a circular microstrip patch antenna will need a large circular aperture with the radius of $0.668\lambda_d$ to operate at the TM$_{31}$ mode. If used in an array configuration, element spacing of $1.336\lambda_d$ would be needed, which results in grating lobes in the visible region. As such, these higher order mode patch elements are rendered ineffective in tightly-spaced antenna arrays for satellites and airborne vehicles, despite their potentials to enhance the resolution for low-elevation satellites. Therefore, there is a need to reduce the size of the patch at this specific mode and bring it close to the dominant mode, which has the smallest area among all the modes. The proposed method in this thesis is based on a geometrical alteration in the patch layer similar to the technique used for the TM$_{21}$ mode in Chapter 3. The technique is inspired by the surface current distributions of the patch antenna at its TM$_{31}$ mode, as illustrated in Fig. 4.3. As it is observed, there exist six distinct peak intensities in the surface current distributions on the circular radiating disk. Therefore, if one places a radial slit in each of these regions where the surface current intensity is maximum, the current path will be meandered, which eventually miniaturizes the antenna size.
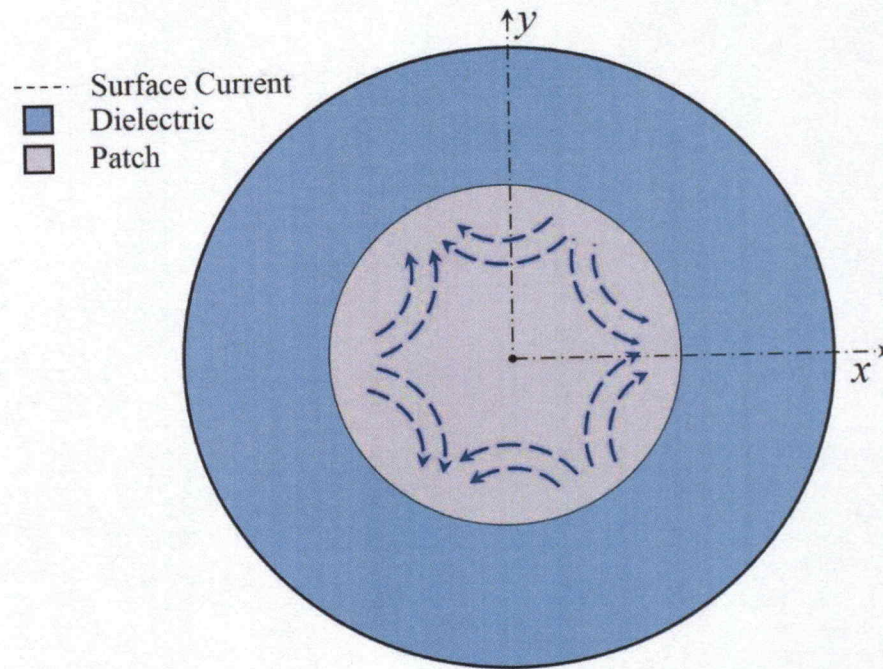
Fig. 4.3: Typical surface current distribution of a circular patch antenna operating at the TM_{31} mode.

The proposed antenna is depicted in Fig. 4.4, where six slits are radially cut from the patch at the maxima of the surface current distributions. The slits are curved trapezoids to intercept the current path as much as possible and are symmetrically arranged with a 60° angular spacing. The slit is defined by its length and angular opening, denoted by L and α, respectively, as shown in Fig. 4.4. These two parameters play a key role in miniaturizing the TM_{31} mode circular microstrip patch antenna.

Similar to the reference antenna, the radius of the patch, denoted by a_{31} in Fig. 4.4, is 26.75 mm, and the ground and substrate have a diameter of 120 mm. Due to the presence of the slits, a slight adjustment needs to be made in the probe location to improve the impedance matching. That is, the 50-Ω coaxial probe is now offset 8.85 mm from the center

of the circular patch. When L=16 mm and α=2°, the resonant frequency of the TM$_{31}$ mode will reduce to about 2.65 GHz, resulting in about 49% reduction in the patch radius. Thus, the proposed miniaturized TM$_{31}$ mode patch antenna now occupies approximately half the aperture size of the unloaded patch, which is remarkable. In addition, this implies that the radius of the miniaturized TM$_{31}$ patch now becomes marginally close to that of the dominant TM$_{11}$ mode. The values of L and α were concluded based on the parametric study, which will be detailed in the following sections.
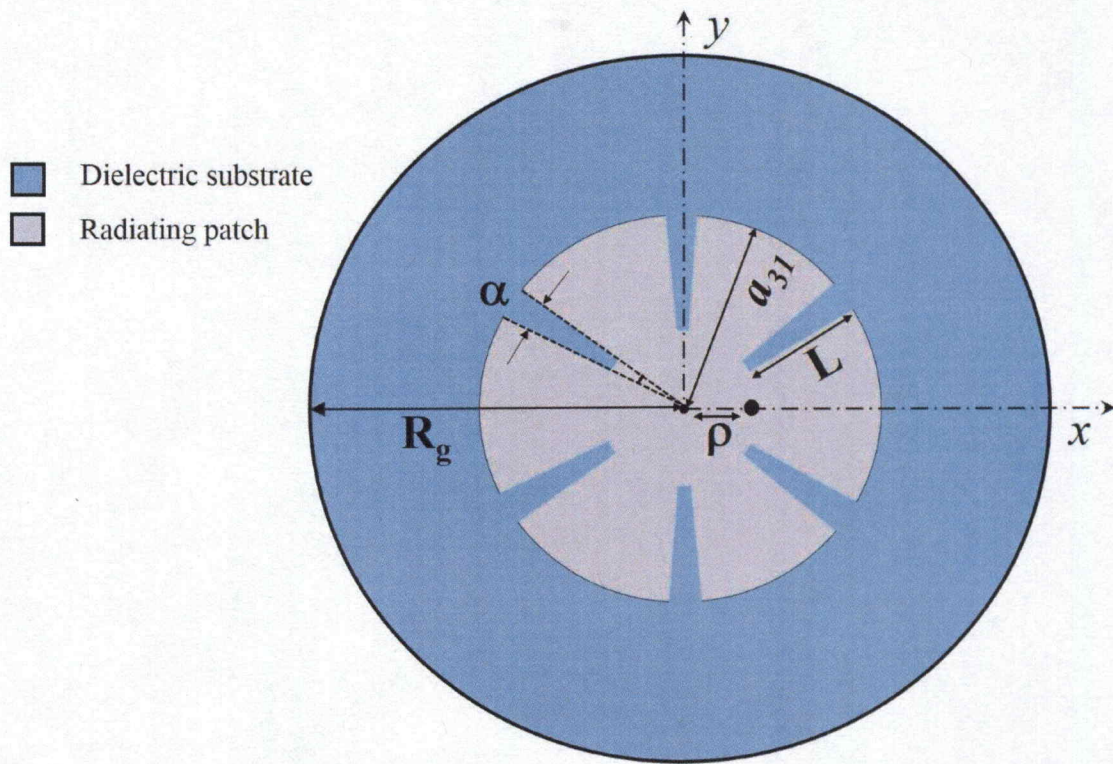
Fig. 4.4: Geometry of proposed slit-loaded TM$_{31}$ circular patch antenna with a_{31} = 26.75 mm, R$_g$ = 60 mm, ρ = 8.85 mm, ε_r = 2.2, and substrate thickness of 1.6mm.

4.4 Effect of the Slits on Antenna Miniaturization

An extensive parametric study has been conducted to finalize the design, resulting in about 49% reduction in the radiating patch radius. In the following sections, the effect of the slit length and slit opening on the resonant frequency of the antenna will be investigated.

4.4.1 Varying Slit Length

In this section, the impact of the slit length, denoted by L in Fig. 4.4, on the resonance frequency is investigated by analyzing the proposed antenna with the finite-element based full-wave electromagnetic solver ANSYS HFSS v.18 [27]. The reflection coefficients are plotted in Fig. 4.5, where L changes from 0 to 16 mm for a fixed α of 2°. As can be seen, the resonant frequencies of the TM_{11}, TM_{21} and TM_{31} modes of the unloaded patch, i.e. the $L=0$ case, occur at 2.17 GHz, 3.62 GHz and 5 GHz, respectively. By placing six symmetrical slits in each of the peak intensities of the surface current distribution on the patch, the resonant frequency of the TM_{31} mode starts decreasing as the slits force the current to meander, helping in increasing the electric size of the patch. Consequently, the resonant frequency shifts down as the slit length increases. As for the TM_{11} and TM_{21} modes, their resonant frequencies are slightly impacted by the slits. More specifically, the resonant frequencies of the TM_{11} mode and TM_{21} mode reduce from 2.17 GHz to 1.76 GHz and 3.62 GHz to 2.42 GHz when $L=0$ and $L=16$mm, respectively. The $|S_{11}|$ is reasonably in the acceptable limit of below -10 dB for different slit lengths for the TM_{31} mode. These modes were numerically confirmed through examining their respective broadside and conical radiation patterns. After extensive studies, it is found that the purity

of the TM_{31} mode will be inversely affected if the slit length exceeds 16 mm, which is mainly due to the presence of other unwanted modes inside the cavity.
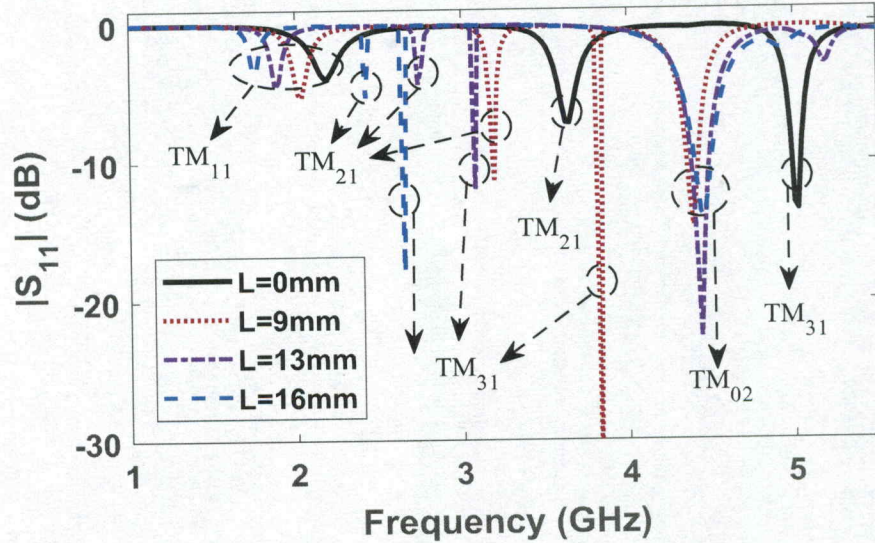
Fig. 4.5: Reflection coefficients of the proposed antenna in Fig. 4.4 for different slit lengths with $\alpha=2°$.

For the TM_{31} mode, a summary of the resonant frequencies, gain, and size reduction of the conventional and miniaturized TM_{31} patch antennas is listed in Table 4.2 for different slit lengths. The resonant frequency of the TM_{31} mode reduces from 5 GHz to 2.65 GHz, resulting in about 49% and 74% reduction in its radius and area, respectively. Similar to other miniaturized antennas, the gain is compromised, as expected. That is, the peak gain drops by about 10.8 dB and 8.8 dB at the E- and H-planes, respectively. In the parametric studies the probe location has been changed by 8.85+/-0.5 mm to compensate for the impedance matching.

Table 4.2: Impact of varying L on resonant frequency, S_{11}, and gain of the slit-loaded patch antenna shown in Fig. 4.4, when $\alpha = 2°$.

L (mm)	Frequency (GHz)	S_{11} (dB)	Gain (dBi)		% reduction of patch radius	% reduction of patch area
			$\phi = 0°$	$\phi = 30°$		
0	5	-13.5	5.27	4.48	N/A	N/A
9	3.82	-14.62	4.84	3.53	26.14%	45.45%
13	3.08	-12	-0.39	-0.68	40.4%	64.5%
16	2.65	-17.91	-5.95	-5.21	**48.74%**	**74%**

4.4.2 Varying Slit Opening

As depicted in Fig. 4.4, each slit has an angular opening which is defined by α. The effect of α on the resonant frequency is investigated in this section. The reflection coefficients are shown in Fig. 4.6 with opening angles varying from $0°$ to $2°$ for a fixed length of $L=16$mm. The parametric study for α was stalled at 2^0 as good impedance matching was not achieved for α greater than 2^0.
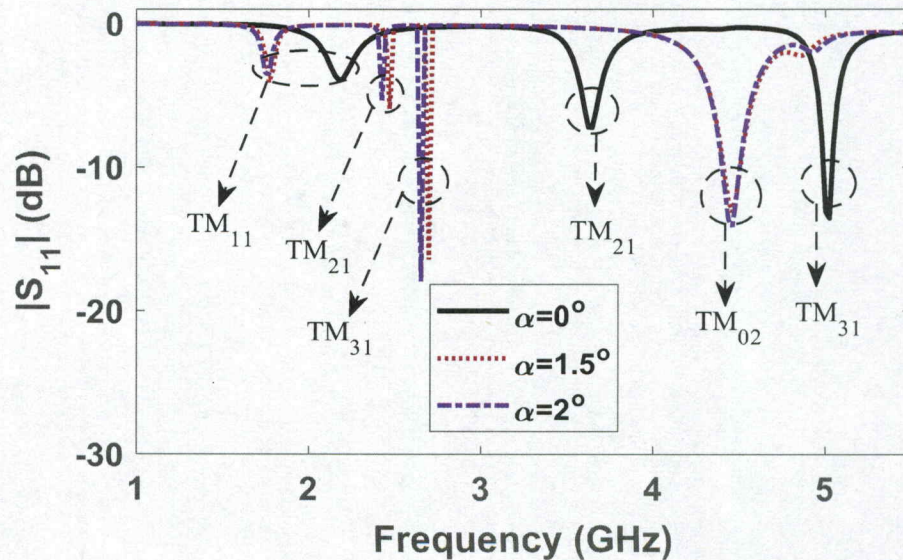
Fig. 4.6: Reflection coefficients of the proposed antenna in Fig. 4.4 for different slit angles with $L=16$mm.

The opening angle (α) provides another degree of freedom to further control the miniaturization. Compared to the length of the slit, the opening angle has lesser influence on the resonance frequency. As it is shown in Fig. 4.6, the resonant frequency of the TM_{31} mode decreases as α increases for the same length. The decrease in resonant frequency due to the change in α is not as significant as varying the length of the slot. The shift in resonance frequency is also seen on the dominant mode of the antenna as well as the TM_{21} mode. Similar to the previous section the gain drops as the antenna is miniaturized by increasing the opening angle of the radial slits. Table 4.3 shows the reduction in area as resonant frequency decreases and miniaturizes the patch size considerably. In the parametric studies the probe location has been changed by 8.85+/-0.5 mm to compensate for the impedance matching.

Table 4.3: Impact of varying α on resonant frequency, S_{11}, and gain of the slit-loaded patch antenna shown in Fig. 4.4, when $L = 16$ mm.

α^o	Frequency (GHz)	S_{11} (dB)	Gain (dBi)		% reduction of patch radius	% reduction of patch area
			$\phi = 0^o$	$\phi = 30^o$		
0°	5	-13.5	5.27	4.48	N/A	N/A
1.5^o	2.69	-16.4	-4.87	-3.52	48.12%	73%
2°	2.65	-17.91	-5.95	-5.21	**48.74%**	**74%**

4.5 Full-Wave Numerical Results

As presented in Section 4.4, the proposed antenna with the finalized slit size of $L = 16$mm and $\alpha = 2^o$ results in about 49% reduction in the patch radius. Thus, it is instructive to further investigate how the antenna performs after miniaturization by comparing its characteristics, including radiation patterns and surface current intensities, with a

conventional TM_{31} patch antenna. In this section, the numerical results of such comparisons are provided.

Fig. 4.7 compares the reflection coefficients of the conventional antenna and the proposed antenna. The resonant frequency of the TM_{31} mode in the slit loaded patch has reduced by almost 49%, equivalent to a 74% reduction in the patch area, which is quite significant. These results are also summarized in Table 4.4 for the TM_{31} mode.

Table 4.4: Reduction in frequency for the unloaded and slit-loaded circular patch antennas at the TM_{31} mode

	Mode	f (GHz)	Radius	χ_{31}	% reduction of patch area
TM_{31}	Before Miniaturization	5	$0.668\lambda_o$	4.20119	-
	After Miniaturization	2.65	$0.354\lambda_o$	2.226	74%
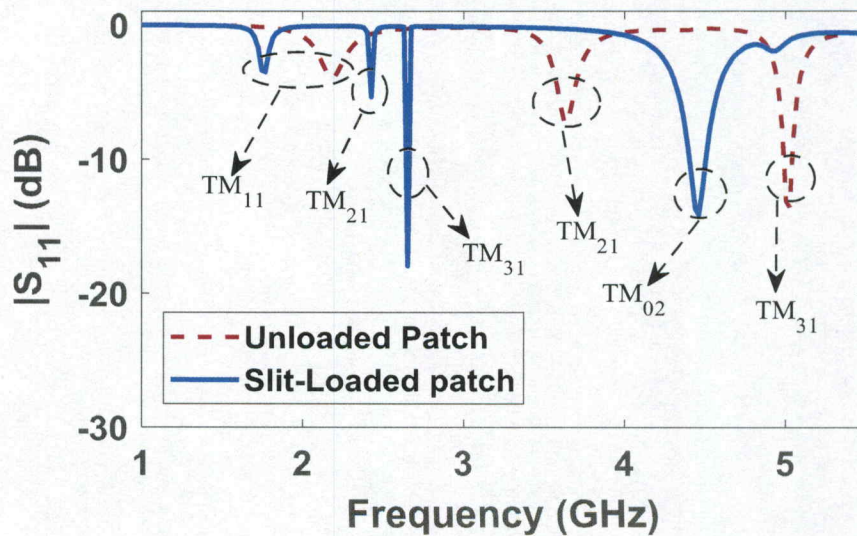
Fig. 4.7: Reflection coefficient of unloaded patch and slit-loaded patch antenna in Fig. 4.4 with L = 16 mm and $\alpha = 2°$.

Radiation patterns of the conventional antenna and the proposed miniaturized antenna are also compared at the TM_{11}, TM_{21} and TM_{31} modes, which are affected by the slits. Fig. 4.8 shows radiation patterns before and after miniaturization for the dominant TM_{11} mode at their respective resonant frequencies of 2.17 GHz and 1.76 GHz. They both have broadside radiation patterns with the peak at the $\theta=0^\circ$ direction, as expected. The shape of the radiation pattern of the dominant mode for the conventional antenna is distorted due to the larger aperture size that can potentially support other higher order mode. After miniaturization, the peak gain of the TM_{11} mode drops by 4.8 dBi and its radiation pattern resumes the standard TM_{11} radiation pattern. To shed light on this, the corresponding surface current distributions of the TM_{11} mode are illustrated in Fig. 4.9, before and after miniaturization at the aforementioned resonant frequencies. After miniaturization, the currents are concentrated in the patch center, resulting in a well-defined broadside pattern with lesser peak gain due to the smaller effective aperture area than the unloaded patch.

Fig. 4.10 shows radiation patterns before and after miniaturization for the TM_{21} mode at their respective resonant frequencies of 3.62 GHz and 2.42 GHz. They both have conical radiation patterns with the null at the $\theta=0^\circ$ direction, as expected. The slits reduce the resonant frequency as they cross the associated surface currents of the mode. The peak gain now drops by about 2.9 dB and 2.7 dB at the E- and H-planes, respectively. For further clarification, the corresponding surface current distributions of the TM_{21} mode are illustrated in Fig. 4.11, before and after miniaturization at the resonant frequencies.

The gain drop is expected to be significant in the case of TM_{31} mode, whose radiation patterns are plotted in Fig. 4.12 before and after miniaturization at their respective

resonant frequencies of 5 GHz and 2.65 GHz. More specifically, the peak gain now drops

by about 11.1 dB and 9.6 dB at the E- and H-planes, respectively. This is mainly attributed

to the fact that the effective aperture area of the antenna becomes much smaller after

miniaturization. As such, the gain is compromised, based on the aperture theory [2]. The

associated surface current distributions are depicted in Fig. 4.13 for the TM_{31} mode before

and after miniaturization. For the latter, the meandered current path is clearly visible around

the radial slits, which subsequently decrease the resonant frequency of the TM_{31} mode

circular patch antenna. The novelty of the proposed design is that the eigenvalue of the

proposed TM_{31} mode is equal to 2.226, which is much smaller than that of a conventional

TM_{31} patch antenna.

(a)   (b)
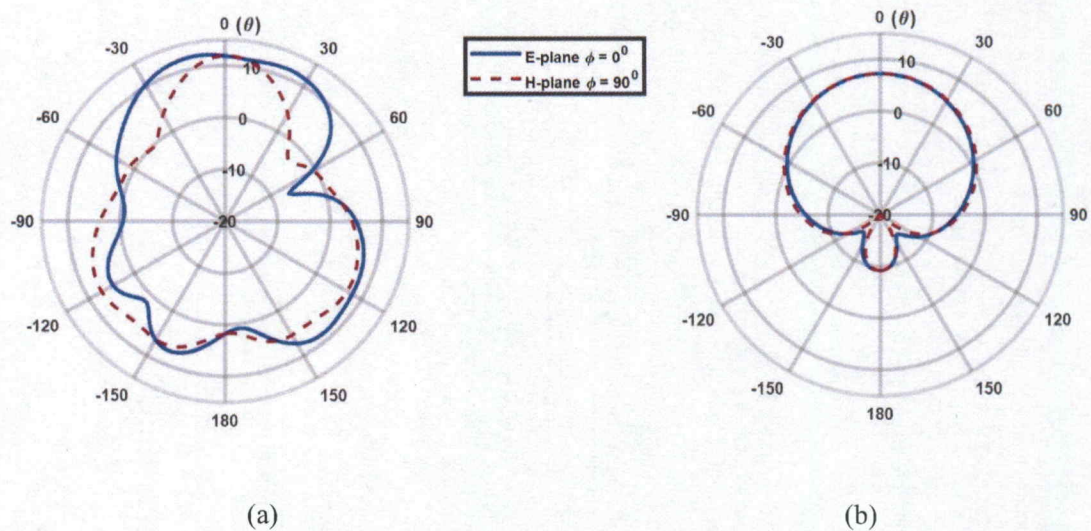
Fig. 4.8: Radiation patterns of the TM_{11} mode for (a) the unloaded patch of $L=0$ and at 2.17 GHz
(b) the proposed antenna in Fig. 4.4 of $L = 16$ mm and $\alpha = 2°$ at 1.76 GHz.
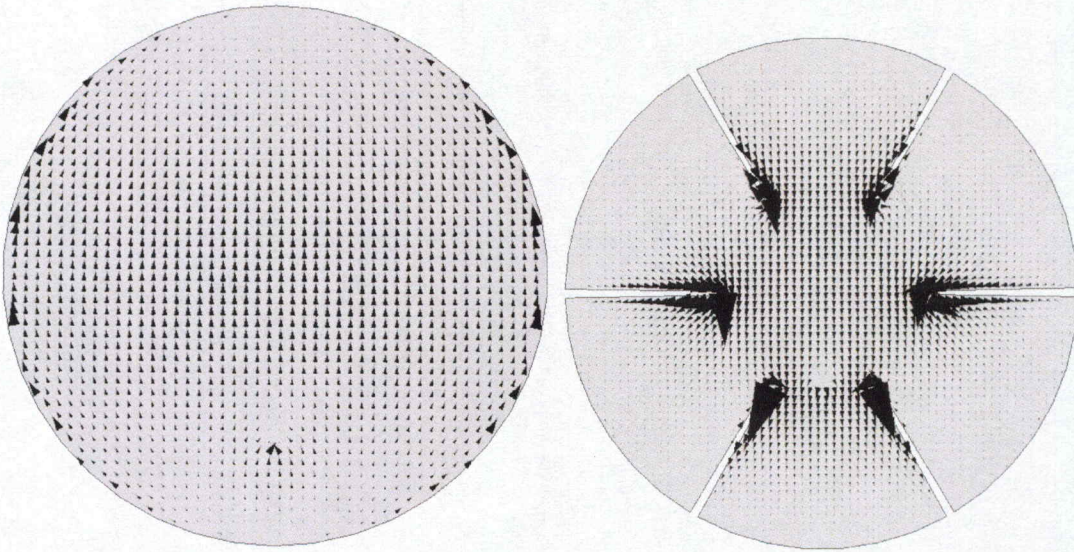
Fig. 4.9: Surface current distributions of the TM_{11} mode for (a) the unloaded patch of $L=0$ and at 2.17 GHz (b) the proposed antenna in Fig. 4.4 of $L = 16$ mm and $\alpha = 2°$ at 1.76 GHz.

(a)   (b)
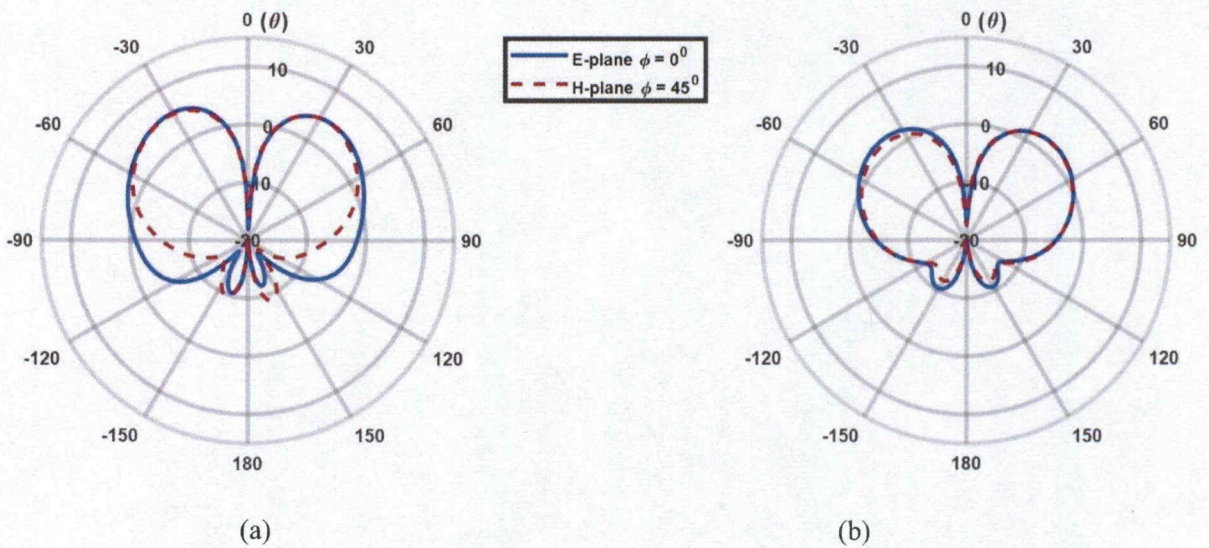
Fig. 4.10: Radiation patterns of the TM_{21} mode for (a) the unloaded patch of L=0 and at 3.62 GHz (b) the proposed antenna in Fig. 4.4 of $L = 16$ mm and $\alpha = 2°$ at 2.42 GHz.
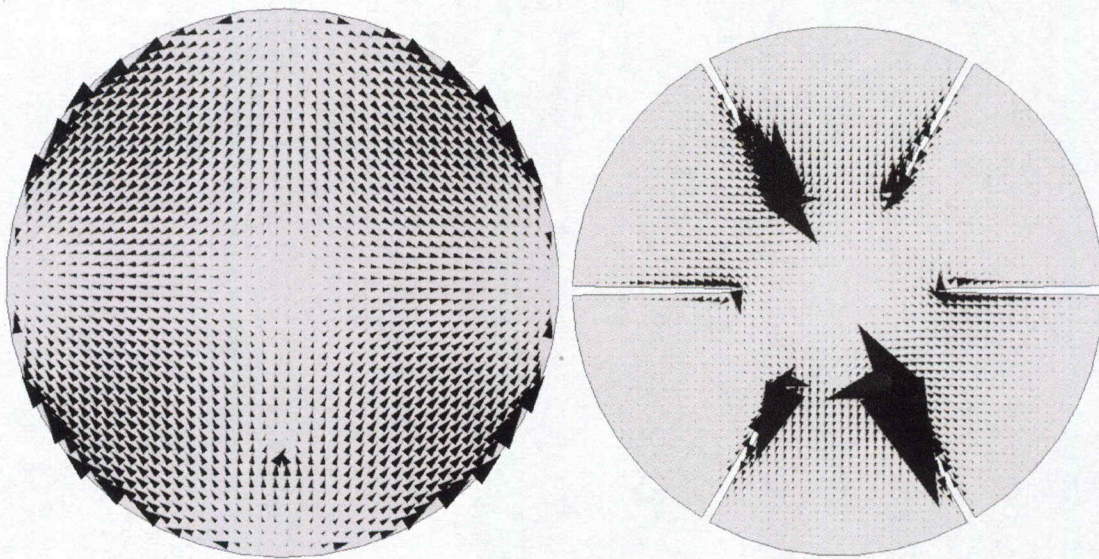
Fig. 4.11: Surface current distributions of the TM_{21} mode for (a) the unloaded patch of L=0 and at 3.62 GHz (b) the proposed antenna in Fig. 4.4 of $L = 16$ mm and $\alpha = 2°$ at 2.42 GHz.

(a)   (b)
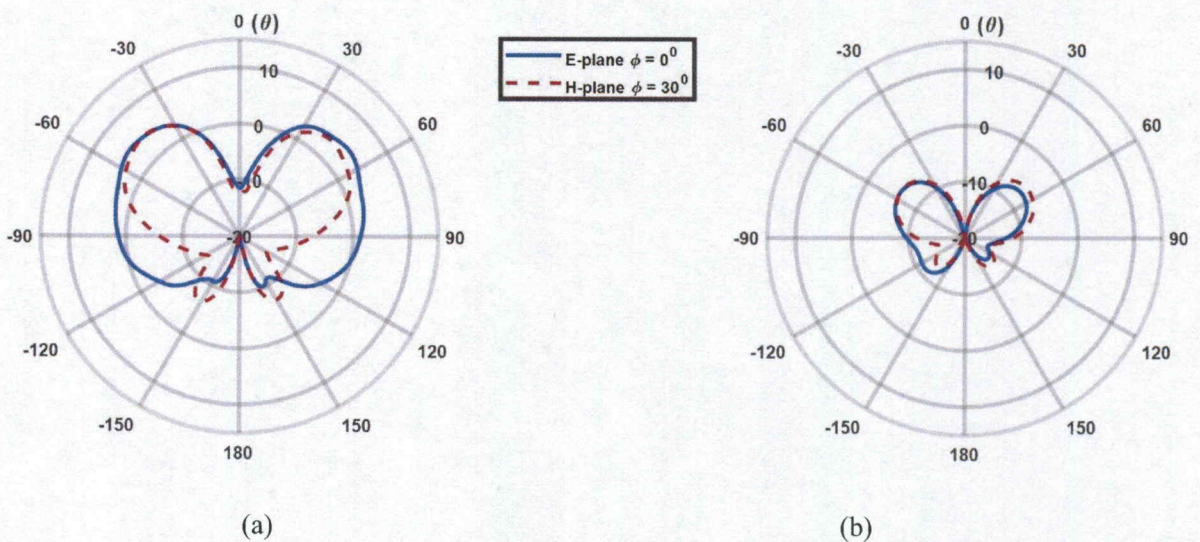
Fig. 4.12: Radiation patterns of the TM_{31} mode for (a) the unloaded patch of L=0 and 5 GHz (b) the proposed antenna in Fig. 4.4 of $L = 16$ mm and $\alpha = 2°$ at 2.65 GHz.
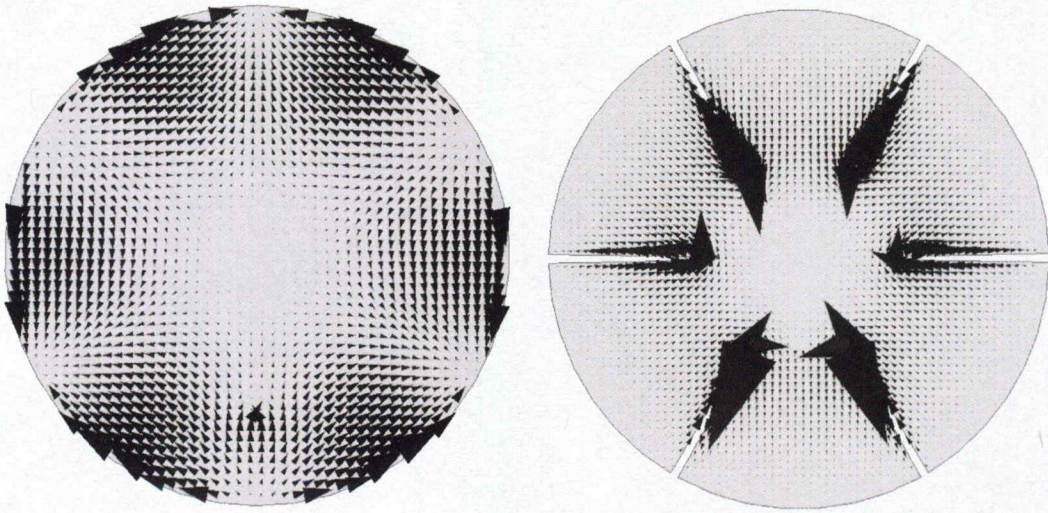
Fig. 4.13: Radiation patterns of the TM_{31} mode for (a) the unloaded patch of L=0 and 5 GHz (b) the proposed antenna in Fig. 4.4 of L = 16 mm and α = 2° at 2.65 GHz.

The three-dimensional radiation pattern of the finalized miniaturized patch antenna with L=16mm and α = 2° is shown in Fig. 4.14 for the TM_{31} mode at the frequency of 2.65 GHz. The peak radiation intensity is clearly scanned and the pattern has a null at the boresight angle of θ=0°, as expected.

53
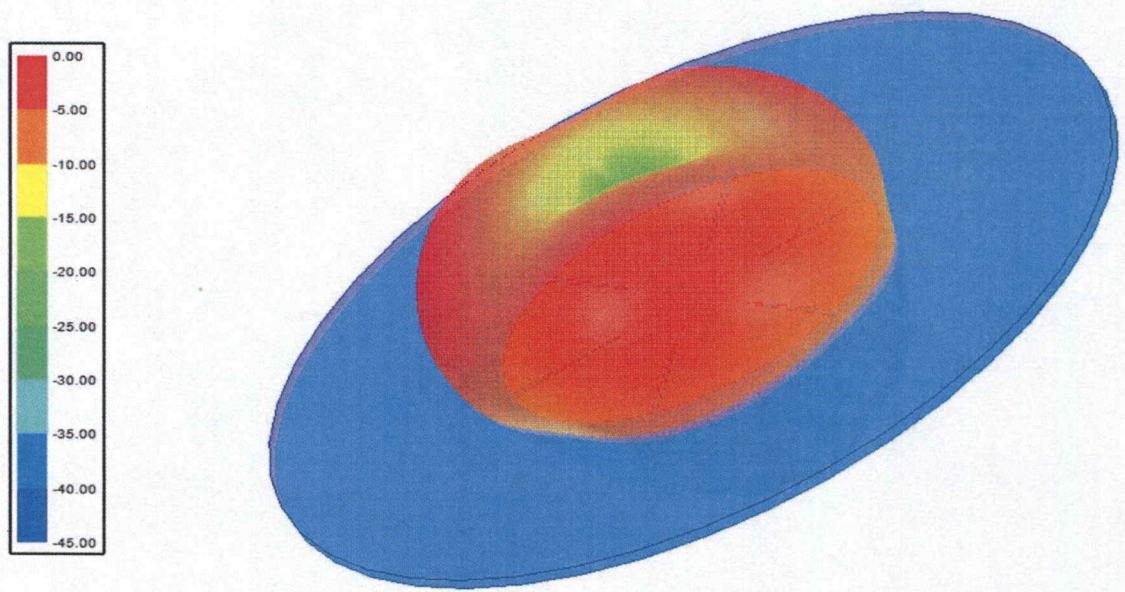
Fig. 4.14: Simulated 3-D radiation pattern of the TM_{31} mode exciting at 2.65 GHz for the proposed miniaturized TM_{31} mode circular patch antenna in Fig 4.4.

4.6 Summary

A novel miniaturized circular patch antenna operating at the TM_{31} mode was introduced. The miniaturization was realized by placing six radial slits to elongate the current path and thus reduce the aperture size of the antenna. A parametric study was conducted to understand the effects of the slits on the size reduction, gain, and reflection coefficients. It was concluded that size of the patch can be controlled by changing the radial and angular dimensions of the slits. Reduction up to 49% and 74% has been achieved in the patch radius and area, respectively, which makes its aperture size comparable to that of the conventional dominant mode. It is also possible to achieve further miniaturization by modifying the slit geometry.

CHAPTER 5

Dual-Band Circular Microstrip Patch Antenna

5.1 Introduction

Other than antennas with conical radiation patterns, presented in Chapters 3 and 4, dual-band antennas are in great demand in wireless communication systems. In particular, it is desired to have stable radiation patterns at two closely-spaced bands with a frequency ratio of close to unity. Such dual-band antennas are capable of improving the signal to noise ratio. This is due to the fact that the frequency bandwidth is broken into two narrower bands, thus limiting the noise at each band. For microstrip patch antennas, a dual-band operation may be realized by different methods, some of which will be reviewed in the following section.

This chapter is focused on designing a compact dual-band microstrip patch antenna operating at the TM_{11} and TM_{12} modes. The objective is to miniaturize the TM_{12} mode circular patch antenna by reducing its eigenvalue from 5.331 close to the eigenvalue of the dominant mode which is 1.8141, while maintaining stable broadside radiation patterns at the two bands. An ideal microstrip patch excited at the TM_{12} mode exhibits broadside radiation patterns with sidelobes present at the either side of the main beam, which reduce the antenna gain. The proposed TM_{12} circular patch antenna design will eliminate the unwanted sidelobes and its radiation pattern will be similar to that of the dominant mode circular patch antenna. The emphasis is placed on generating a dual-band microstrip patch antenna with a frequency ratio close to unity.

5.2 Review of Dual-Band Patch Antennas with Broadside Patterns

Multi-band antennas with identical radiation patterns and polarization on a single-layer structure are highly desirable in airborne platforms such as synthetic aperture radar (SAR), which requires lightweight and low cost multi-band antennas for satellite links and wireless networks [23]. An earlier study in dual-band antennas was carried out in rectangular microstrip patch antennas [28]. S. Maci et al. [29] designed a rectangular microstrip patch antenna operating at the TM_{30} mode. The proposed antenna consisted of two narrow slots close to the radiating edges of the antenna patch. The lower modes showed negligible reduction in frequency with the addition of the slots to the conventional antenna. There was a considerable reduction in the resonant frequency of the TM_{30} mode. The obtained frequency ratio was between 1.6 and 2 by employing the slots. Additionally, the authors decreased the frequency ratio within a range of 1.1 and 1.4 for global positioning system (GPS) and radar applications using matching stubs connecting the ground plane and the radiating patch between the slots. The stubs affected the radiation pattern and brought ohmic losses to the antenna, which subsequently degraded the efficiency of the antenna as the frequency ratio decreased.

The slot loading technique used in rectangular patch antennas was applied to circular patch antennas by Kin-Lu Wong and Gui-Bin Hsieh [30], who designed radial arc-shaped slots symmetrical to the center of the radiating circular patch. The arc-shaped slots were natural modifications to the slots used by Maci [29] and were employed with an objective to reduce the frequency ratio between the TM_{11} and TM_{12} modes. A study was carried out to decrease the frequency ratio with the help of the subtending angle of the arc shaped slots. The observations from the parametric study demonstrated that as the angle

increased from 80° to 100°, the frequency ratio reduced from 1.58 to 1.38. The radiation patterns illustrated in [30] were nearly identical to an ideal broadside radiation pattern. The design can be used in applications requiring dual frequency operation with broadside radiation patterns.

In [31], an inset-microstrip-line-fed dual frequency circular microstrip antenna with a single arc-shaped slot was proposed with a tunable frequency ratio of 1.29 to 1.43 between its dominant mode and the TM_{12} mode. The reported radiation patterns of the TM_{11} and TM_{12} modes were broadside with identical polarization planes at the resonant frequencies. The frequency ratio can be varied by altering the length of the arc-shaped slot on the radiating patch, which controls the resonant frequency of the TM_{12} mode. The work was extended to a two-element dual frequency microstrip array for base station applications [31]. The drawback of the work is the unwanted sidelobes present in the radiation pattern in the E-plane, which reduces the gain of the antenna in the targeted broadside region.

5.3 Analysis of the TM_{12} Circular Microstrip Patch Antenna

As listed in Table 2.1, the associated eigenvalue of the TM_{12} mode, i.e. χ_{12}, in a circular microstrip patch antenna is 5.331. Thus, based on the cavity model described in Chapter 2, the radius of the TM_{12} mode circular patch is determined by the following equation [4]:

$$a_{12} = \frac{5.331 \lambda_o}{2\pi\sqrt{\varepsilon_{eff}}} = 0.848 \lambda_d \qquad (5.1)$$

where ε_{eff} is the effective dielectric constant due to the fringing electric fields and λ_d is the dielectric wavelength, expressed by,

$$\lambda_d = \frac{c}{f\sqrt{\varepsilon_{eff}}} \tag{5.2}$$

where C is the speed of light in free space and f is the operating frequency of the antenna, which is 5 GHz for the conventional TM_{12} mode patch antenna under study in this chapter. As presented in Chapter 2 using the cavity model assuming an infinite ground plane, the spherical components of the radiated electric fields are given by the following equations for a circular patch antenna of radius a_{12} operating at the TM_{12} mode at the far-field region [7]

$$E_\theta = j\frac{Va_{12}\kappa_o}{4}\frac{e^{-j\kappa_o r}}{r}\left(J_2(\kappa a_{12}\sin(\theta)) - J_0(\kappa a_{12}\sin(\theta))\right)\cos\phi \tag{5.3}$$

$$E_\phi = j\frac{Va_{12}\kappa_o}{4}\frac{e^{-j\kappa_o r}}{r}\cos\theta\left(J_2(\kappa a_{12}\sin(\theta)) + J_0(\kappa a_{12}\sin(\theta))\right)\sin\phi \tag{5.4}$$

Unlike the TM_{21} and TM_{31} modes with conical radiation patterns presented in Chapters 3 and 4, the TM_{12} mode generates broadside radiation patterns, similar to the TM_{11} mode. This is illustrated in Fig. 5.1, where typical far-field radiation patterns for the TM_{12} mode circular patch mounted on an infinite ground plane are plotted. Similar to the dominant TM_{11} mode, the pattern is broadside with the main beam located at the boresight direction of $\theta = 0°$, however it has unwanted sidelobes at the E-plane. These sidelobes are due to the nulls in the surface current distributions beyond the TM_{11} mode region of the patch, as depicted in Fig. 5.2.
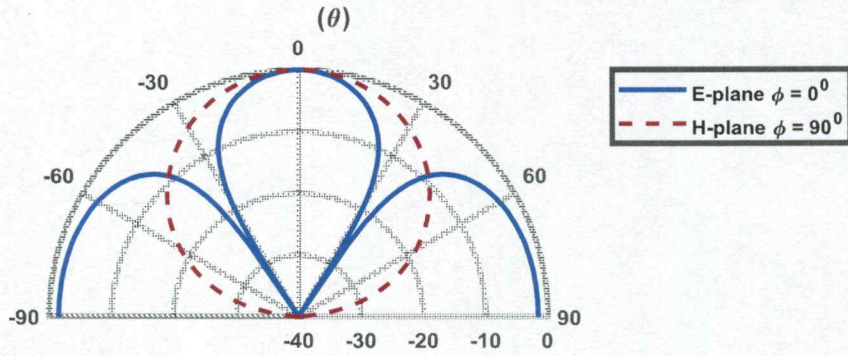
Fig. 5.1: Typical far-field radiation patterns of a TM_{12} mode circular patch antenna with $a_{12}=0.848\lambda_d$, backed by an infinite ground plane.

Compared to the previous cases of TM_{21} and TM_{31} modes, where the patch has null at the center, the TM_{12} mode now possesses two distinct nulls in the form of two narrow arcs away from the patch center. These nulls only exist along the E-plane, i.e. the plane parallel to the electric field, and thus create unwanted sidelobes along the E-plane, as shown in Fig. 5.1. Therefore, in order to have stable broadside patterns at the two modes, the unwanted sidelobes need to be eliminated properly. One way to mitigate this is to place two narrow arc slots in the vicinity of the aforementioned nulls, as reported in [30]. Similar to the miniaturized TM_{21} and TM_{31} modes, this will increase the electrical length of the TM_{12} mode and as such the resonant frequency will decrease. It should be noted that since the arc slots are placed outside the TM_{11} mode region, the resonant frequency of the dominant TM_{11} mode will be almost unchanged. Therefore, the arc slit method simultaneously addresses the unwanted sidelobes of the TM_{12} mode and brings its resonant frequency close to that of the TM_{11} mode, resulting in a dual-band antenna with stable broadside radiation patterns.

59
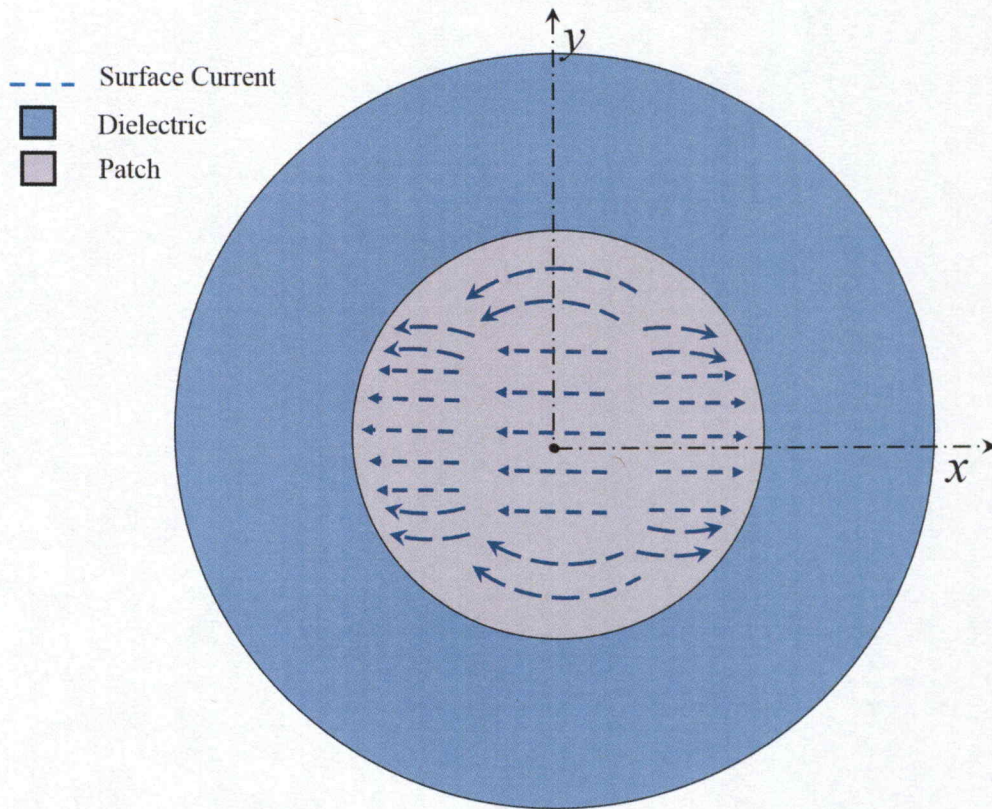
Fig. 5.2: Typical surface current distribution of a conventional TM_{12} mode circular microstrip patch antenna.

In this chapter, the reference case is a conventional microstrip patch antenna at the TM_{12} mode, whose geometry is depicted in Fig. 5.3, and it is designed to resonate at 5 GHz. For practical applications, a truncated ground plane size that is sufficiently large to reduce the back radiation needs to be used. As such, the reference TM_{12} patch is mounted on a circularly shaped grounded dielectric slab with a diameter of 150 mm. The radius of the patch, denoted by a_{12} in Fig. 5.3, is 33.25 mm. The antenna is fed by a 50-Ω coaxial probe with a feed point offset 6 mm from the center of the circular patch. The substrate is RT Duroid 5880 [25] with ε_r=2.2 and a thickness of 1.6 mm. The design specifications of the reference TM_{12} mode circular patch antenna are given in Table 5.1.

Table 5.1: Design specification of a circular microstrip patch antenna operating at the TM_{12} mode.

Design Parameters	Design values
Frequency	5 GHz
Height of the substrate (h)	1.6 mm
ε_r	2.2
Loss Tangent	0.0009
Substrate Material	RT Duroid 5880
Radius of the patch (a_{12})	33.25 mm
Radius of the ground (R_g)	75 mm
Probe feed from the center (ρ)	6 mm
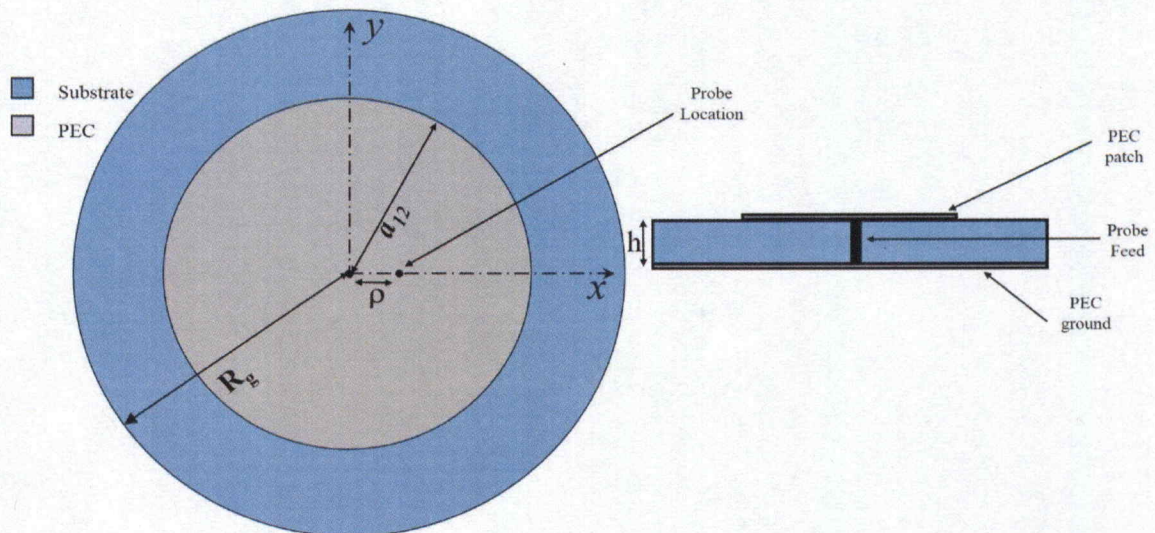
Fig. 5.3: (a) Top- and (b) side-view of a conventional TM_{12} mode circular patch antenna at 5 GHz with $a_{12} = 33.25$ mm, $R_g = 75$ mm, $\rho = 6$ mm, and h = 1.6 mm.

It will be shown that a dual-frequency operation with a small frequency ratio can be obtained using the arc slot-loading technique in a circular microstrip antenna, supporting both TM_{11} and TM_{12} modes. The antenna design and the resonant modes of the proposed

61

dual-band antenna are described, and parametric studies are conducted to understand the effects of arc dimensions on the dual-frequency performance of the antenna.

5.4 Parametric Study of Pre-Designed Antenna

The proposed antenna in this chapter is inspired by the design reported in paper [30] with a frequency ratio of 1.38. First, attempts are made to further reduce the frequency ratio from the reported ratio of 1.38. An extensive parametric study is conducted to finalize the arc dimensions, further reducing the frequency ratio to 1.27. In this section, the effect of arc-slot dimensions is investigated on the resonant frequencies of the antenna.
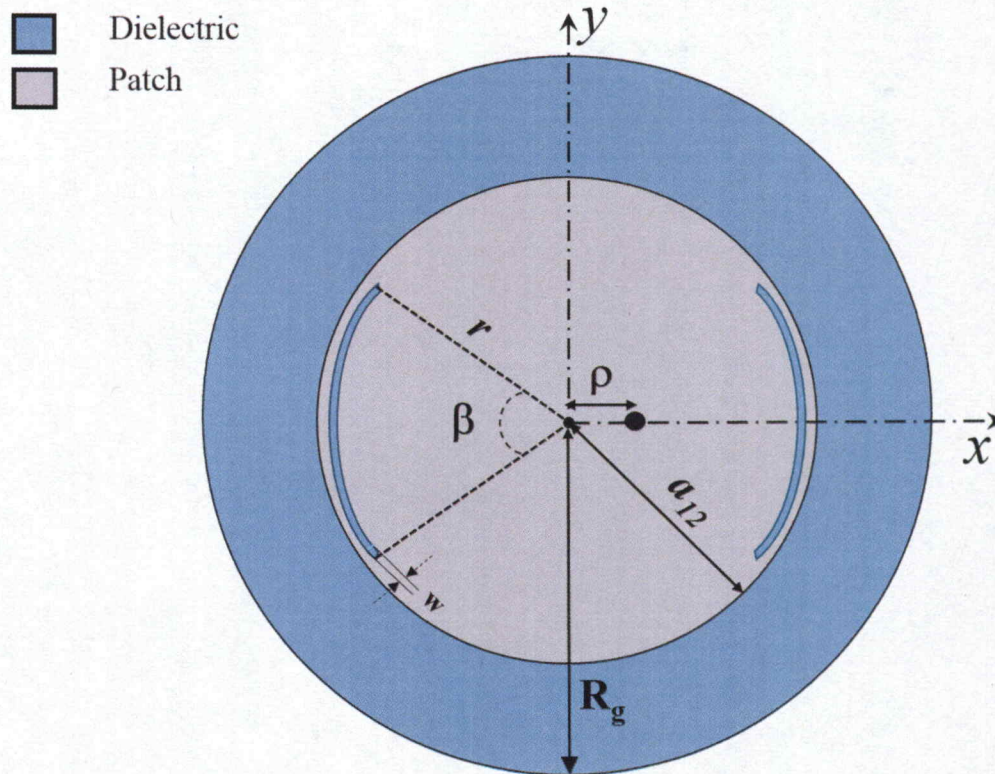
Fig. 5.4: Geometry of arc slit-loaded TM_{12} circular patch antenna: $a_{12} = 33.25$mm; $R_g = 75$mm, ρ=8.5 mm, ε_r=2.2, and substrate thickness of 1.6mm without the extensions to the proposed arc slots.

Fig. 5.4 is the redesigned structure of the antenna proposed in [30]. The arcs are placed closer to the patch circumference to not disturb the surface currents associated with the TM_{11} mode. Each arc is defined by its radius, subtended angle, and width, denoted by r, β, and w, respectively, as shown in Fig. 5.4. The reflection coefficients are plotted in Fig. 5.5, when β changes from 55° to 105° for w= 0.8mm and r = 32.25mm.
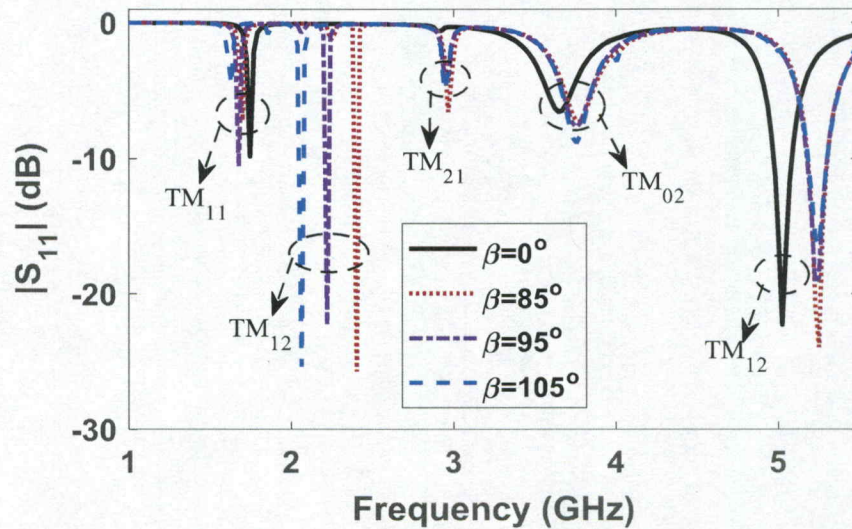
Fig. 5.5: Reflection coefficients of the antenna geometry in Fig. 5.4 for different β with w=0.8mm and r=32.25 mm.

As can be seen, the resonant frequencies of the TM_{11} and TM_{12} modes of the unloaded patch, i.e. the β=0° case, occur at 1.74 GHz and 5 GHz, respectively. The TM_{11} and TM_{12} modes were numerically confirmed through examining their broadside radiation patterns without and with sidelobes, respectively. A considerable reduction in the resonant frequency of the TM_{12} occurs from 5 GHz to 2.1 GHz when β = 105°. The resonant frequency of the TM_{11}, on the other hand, slightly reduces from 1.74 GHz to 1.65 GHz. For the re-designed patch antenna, the frequency ratio between the dominant mode and TM_{12} mode reduces from the reported ratio of 1.38 in [30] to 1.27. Table 5.2 presents the

data from the parametric study. The gain of the antenna at the TM_{12} mode increases as the resonance frequency decreases, due to the eliminated sidelobes at the E-plane.

Table 5.2: Parametric study of the antenna in Fig. 5.4 with different opening angle, when w=0.8mm and r=32.25mm.

β	Frequency for TM_{12}(GHz)	Frequency for TM_{11}(GHz)	Gain for TM_{12} (dBi)	Frequency ratio
0°	5	1.74	7.36	2.87
85°	2.4	1.65	8.68	1.45
95°	2.22	1.65	8.92	1.34
105°	**2.06**	**1.62**	**9.35**	**1.27**

As depicted in Fig. 5.4, the width of the arc slots is defined by w. The effect of the width of the arc is investigated on the resonant frequency. The reflection coefficients are shown in Fig. 5.6 when the widths varies from 0.8 to 1.8 for a fixed β = 105° and r=32.25mm
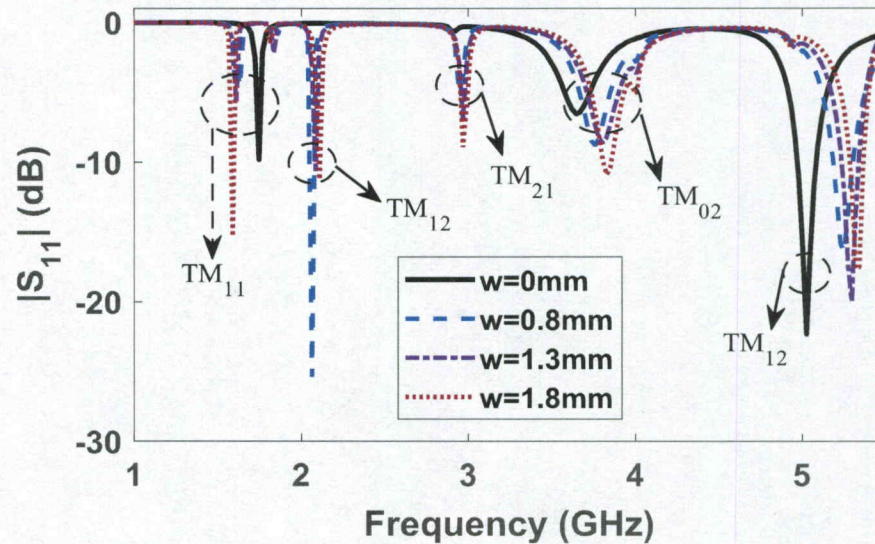
Fig. 5.6: Reflection coefficients of the antenna geometry in Fig. 5.4 for different w with a constant β=105° and r=32.25mm.

From Fig. 5.6, it can be observed that there is an inconsequential reduction to the resonant frequency. Alteration in the width of the arcs does not contribute to the miniaturization of the antenna significantly as demonstrated in the reflection coefficients plotted in Fig. 5.6. This is due the fact that the width considered in the proposed antenna is very small compared to the wavelength of the antenna. Therefore, the width of the arcs does not play a major role in miniaturization as β. Minute fabrication errors with respect to the width can be tolerated.

In contrast, the position of the arc on the circular patch is expected to further miniaturize the TM_{12} mode and reduce its resonant frequency. As depicted in Fig. 5.4, the arc position is controlled by its radius r, i.e. the distance from the patch center to the outer ring of the arc. Fig. 5.7 shows the reflection coefficients, when r changes from 27.25 mm to 32.25 mm.
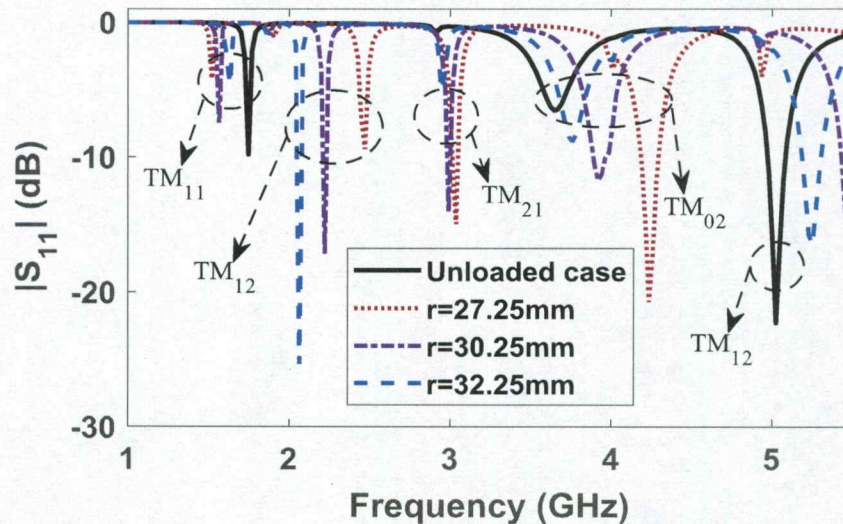

Fig. 5.7: Reflection coefficients of the antenna in Fig. 5.4 for different r with w=0.8mm and β=105°.

65

As observed in Fig. 5.7, the resonant frequency of the TM_{12} mode decreases as the arcs move toward the patch edge. This is because the surface currents associated with the TM_{12} that are close to the patch edge are meandered by the arcs and subsequently the resonant frequency decreases. As for the TM_{11} mode, since its associated surface currents are mostly populated in the center of the patch, its resonant frequency is slightly impacted by the arcs. A summary of resonant frequencies and the TM_{12} gain is provided in Table 5.3. To further reduce the frequency ratio, the antenna reported in [30] needs to be accordingly modified, as detailed in Section 5.5.

Table 5.3: Parametric study of the antenna in Fig. 5.4 with different arc radii, when w= 0.8mm and β= 105°.

r (mm)	Frequency for TM_{12}(GHz)	Frequency for TM_{11}(GHz)	Gain for TM_{12} (dBi)	Frequency ratio
Unloaded case	5	1.74	7.36	2.87
27.25	2.46	1.7	8.08	1.44
30.25	2.22	1.65	8.63	1.34
32.25	2.06	1.62	9.35	1.27

5.5 Proposed TM_{12} Circular Microstrip Patch Antenna

The TM_{12} mode microstrip circular patch antenna requires a larger aperture area than the antennas operating at the lower order modes, as discussed in previous chapters.

As seen in Fig. 5.2, an ideal TM_{12} circular microstrip patch has surface current distributions similar to the dominant mode at its central region, which is enclosed by two nulls and a ring. These nulls will create an unwanted sidelobes in the E-plane radiation pattern, as depicted in Fig. 5.3. Hence, the antenna pattern gets disturbed between the main lobe and the two sidelobes formed at lower elevation angles. To mitigate these unwanted sidelobes as well as decrease the resonant frequency of the TM_{12} mode and bring it close

to that of the TM_{11} mode, the arc-shaped slot loaded technique reported in [30] was further optimized, reducing its frequency ratio from 1.38 to 1.27. In this section, further attempts are made to lower the reported frequency ratio of 1.38, while simultaneously retaining well-defined broadside radiation patterns for both TM_{11} and TM_{12} modes.

In order to decrease the frequency ratio of the TM_{12} to TM_{11} modes and maintain their broadside radiation patterns, the geometry of the arc slots are modified. In particular, the arc ends are radially extended toward the patch center, to provide more room for further meandering the TM_{12} currents and thus reducing its resonant frequency. At the same time, the amount of such extensions should be small enough to not interfere with the associated currents for the TM_{11} mode. This is numerically investigated by performing parametric studies on the length of these extra radial extensions in the arcs. The proposed antenna is illustrated in Fig. 5.8, wherein the radial extensions are defined by L.

The antenna parameters are kept unchanged. That is, the radius of the patch denoted by a_{12} in Fig. 5.8 is 33.25 mm, fed by a 50-Ω coaxial probe with a feed point offset 8.5 mm from the center of the circular patch. The ground and substrate have a diameter of 150 mm. When $\beta=105°$, $w=2°$ and $L = 6$ mm, the resonant frequency of the TM_{12} mode will decrease to about 1.92 GHz. The values of w, L and β were concluded based on the parametric study as will be shown in the following section.
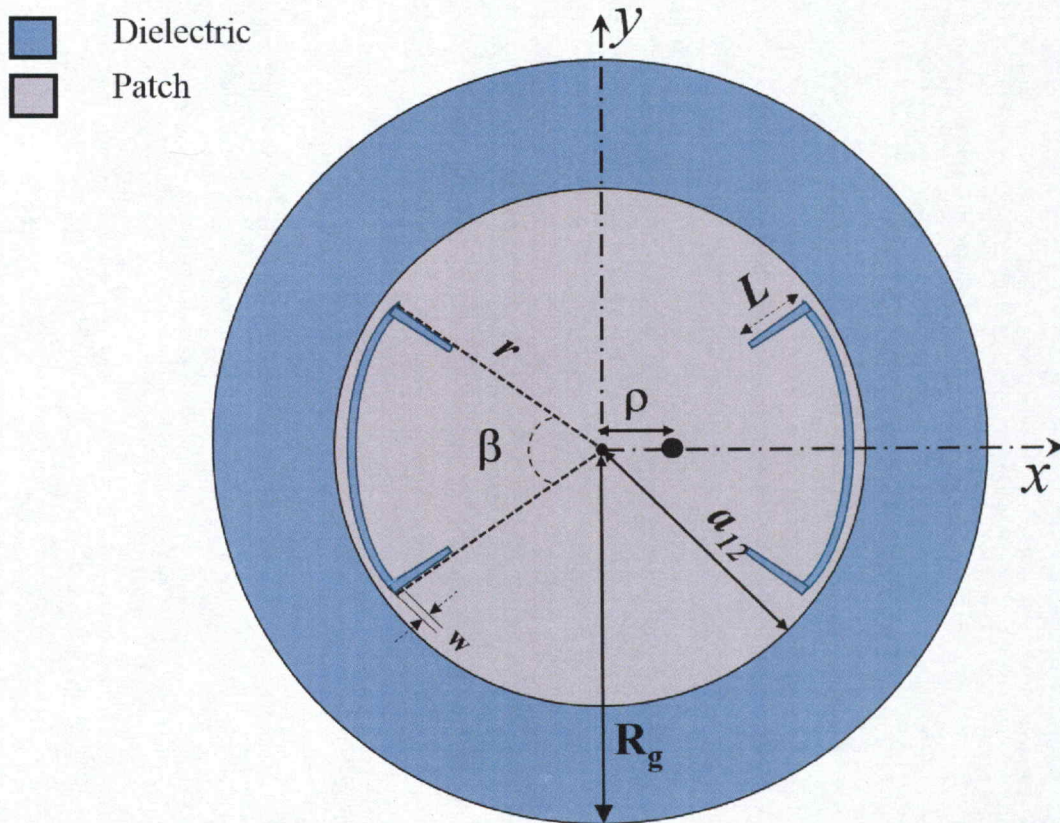
Fig. 5.8: Geometry of proposed slit-loaded TM_{12} circular patch antenna: $a_{12} = 33.25$mm, r=32.25mm, R_g = 75mm, ρ=8.5 mm, ε_r=2.2, and substrate thickness of 1.6mm.

5.6 Full-Wave Numerical Results

A parametric study is conducted to finalize the design, resulting in a frequency ratio of 1.21, which is smaller than the previously reported in [30]. The effect of slot length on the resonance frequencies of the TM_{11} and TM_{12} modes is studied in this section.

The frequency ratio now reaches to 1.13. The reflection coefficients for the parametric study are shown in Fig. 5.9, when L varies from 0mm to 9mm.
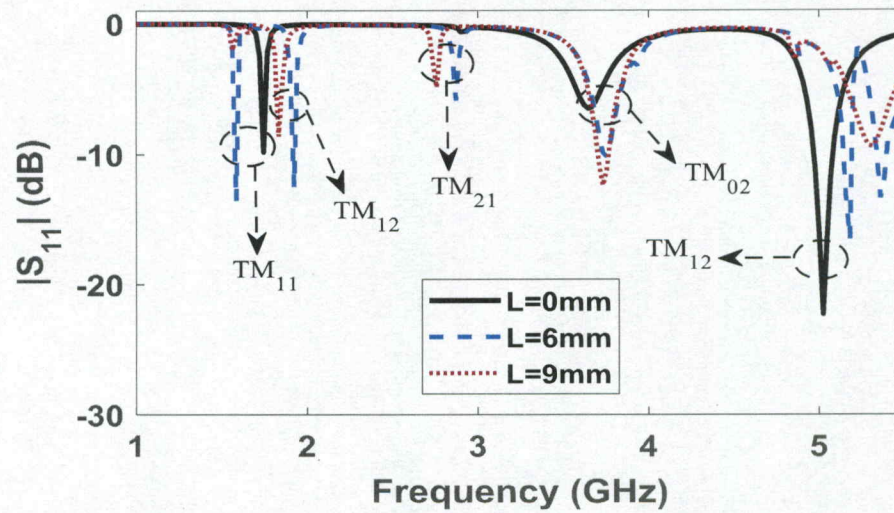
Fig. 5.9: Reflection coefficients of the antenna geometry in Fig. 5.8 for different L with a constant r=32.25mm, w=0.8mm and β=105°.

From the reflection coefficients shown in Fig. 5.9 it is observed that as L increases a reduction in the TM_{12} resonant frequency is observed, whereas the TM_{11} mode slightly changes. Subsequently, the frequency ratio between TM_{11} and TM_{12} decreases. The drawback in having longer rectangular extensions is that the slots start interfering with the surface current distributions associated with the TM_{11} mode which are present in the center of the patch. Table 5.4 summarizes the results and shows that the gain increases with a decrease in resonating frequency as the sidelobes are eliminated similar to the parametric analysis conducted in Section 5.2.2. The increase in gain in this section is not as high as the previous section, as the antenna is highly miniaturized.

Table 5.4: Parametric study of the antenna in Fig. 5.8 with different length, when w= 0.8mm, r=32.25mm and β= 105°.

L (mm)	Frequency for TM_{12}(GHz)	Frequency for TM_{11}(GHz)	Gain for TM_{12} (dBi)	Frequency ratio
0	5	1.74	7.36	2.87
6	1.92	1.58	8.08	1.21
9	1.83	1.61	7.9	1.13

Fig. 5.10 shows the reflection coefficients of the finalized slit-loaded antenna and the reference patch. It is observed that the resonant frequency has decreased considerably from 5 GHz to 1.92 GHz for the TM_{12} mode. A less significant reduction in frequency can also be observed in the TM_{11} mode, whose frequency has decreased from 1.72 GHz to 1.58 GHz. Thus, the designed slots have impacted the TM_{12} more than the other modes. The final length (L), opening angle (β) and width (w) are 6mm, 105°, and 0.8mm, respectively.
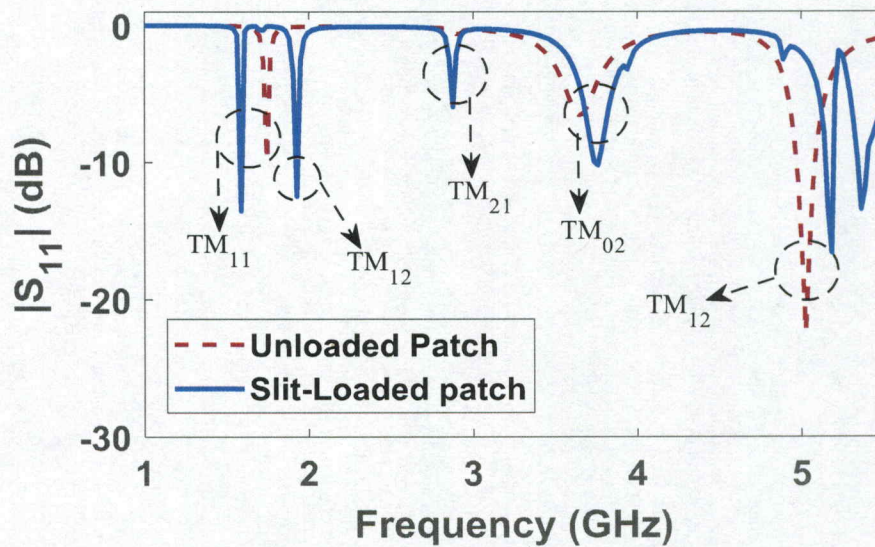
Fig. 5.10: Reflection coefficients of unloaded patch and loaded patch shown in Fig. 5.8 with L=6mm, r=32.25mm, β=105°, and w=0.8mm.

Radiation patterns of the conventional antenna and the proposed antenna are also compared at excited modes, i.e. TM_{11} and TM_{12} modes, which are affected by the arc-slots. They are plotted in Figs. 5.11 and 5.13 for the TM_{11} and TM_{12} modes, respectively. Their corresponding surface current distributions are illustrated in Figs. 5.12 and 5.14, which clearly show the effects of the arcs on the different modes at their respective frequencies. The TM_{11} mode retains its broadside radiation pattern at 1.72 GHz in the unloaded case and 1.58 GHz in the loaded case. The TM_{12} mode also has a broadside radiation pattern

similar to the dominant mode. However, the unloaded patch has sidelobes due to the nulls on the patch around the center. The arcs force the nulls towards the periphery of the patch and eliminate the sidelobes from the radiation pattern. The surface currents associated with the TM_{12} mode meander around the arcs, decreasing the frequency of the TM_{12} mode.

Fig. 5.11: Radiation patterns of the TM_{11} mode (a) at 1.74 GHz for the unloaded patch and (b) at 1.58 GHz when L=6mm and β = 105° for the proposed antenna geometry in Fig. 5.8.
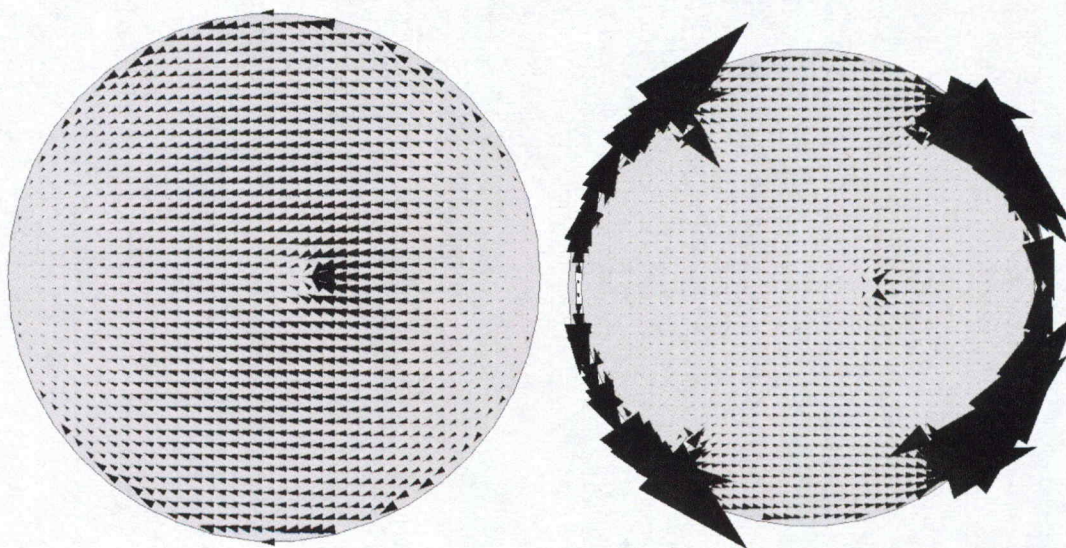
Fig. 5.12: Surface current distributions of the TM_{11} mode (a) at 1.74 GHz for the unloaded patch and (b) at 1.58 GHz when L=6mm and β = 105° for the proposed antenna geometry in Fig. 5.8.

71
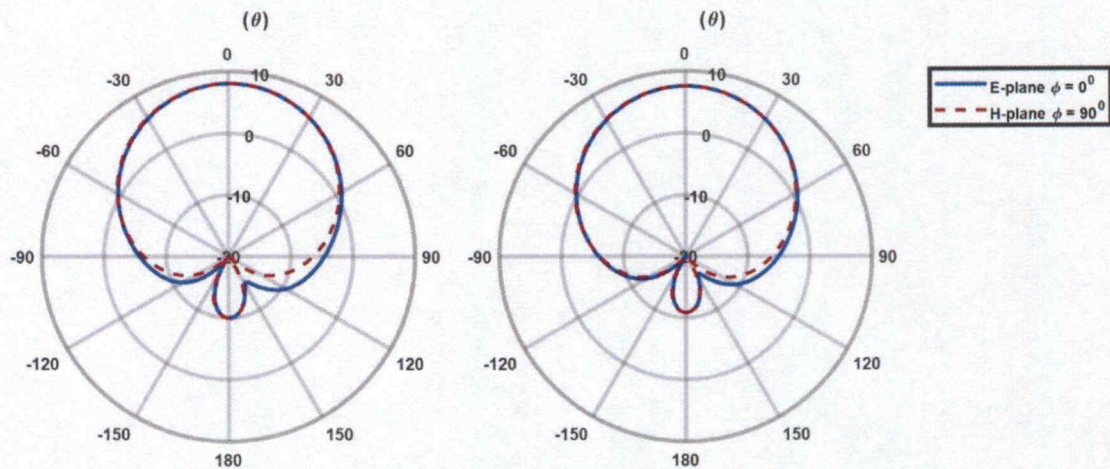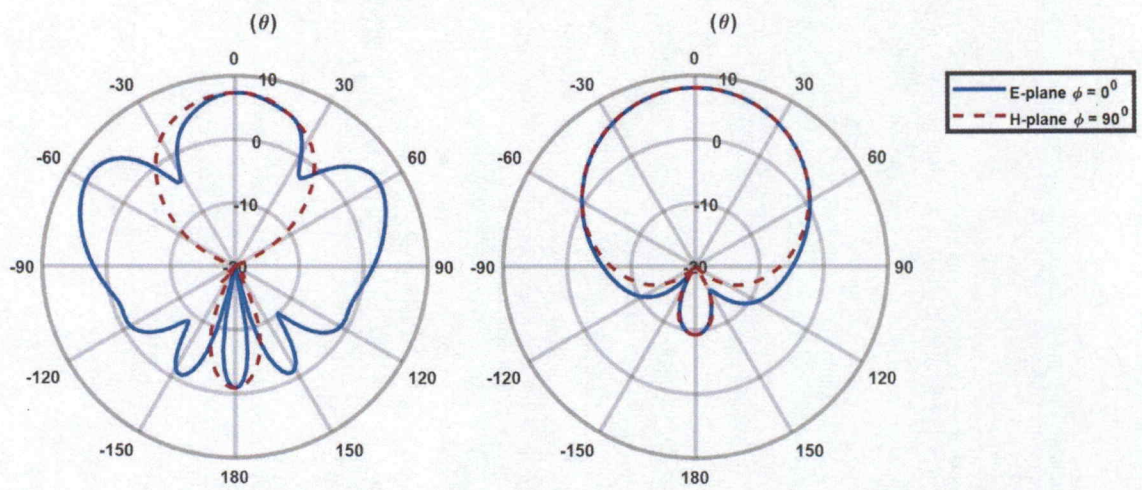
Fig. 5.13: Radiation patterns of the TM_{12} mode (a) at 5 GHz for the unloaded patch and (b) at 1.92 GHz when L=6mm and β = 105° for the proposed antenna geometry in Fig. 5.8.
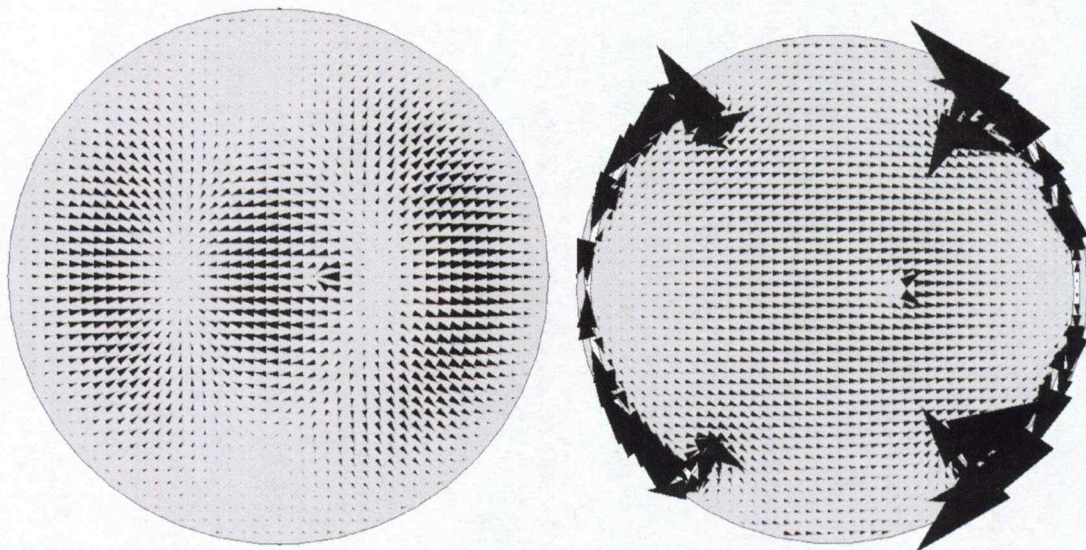
Fig. 5.14: Surface current distributions of the TM_{12} mode (a) at 5 GHz for the unloaded patch and (b) at 1.92 GHz when L=6mm and β = 105° for the proposed antenna geometry in Fig. 5.8.

The three-dimensional radiation pattern of the finalized miniaturized patch antenna with L=6mm and β= 105° is shown in Fig. 5.15 for the TM_{12} mode at the frequency of 1.92 GHz. The peak radiation intensity is clearly visible at the boresight region and is free from any sidelobes. The similarity between the radiation patterns of TM_{11} and TM_{12} mode make this a dual-band circular patch antenna.
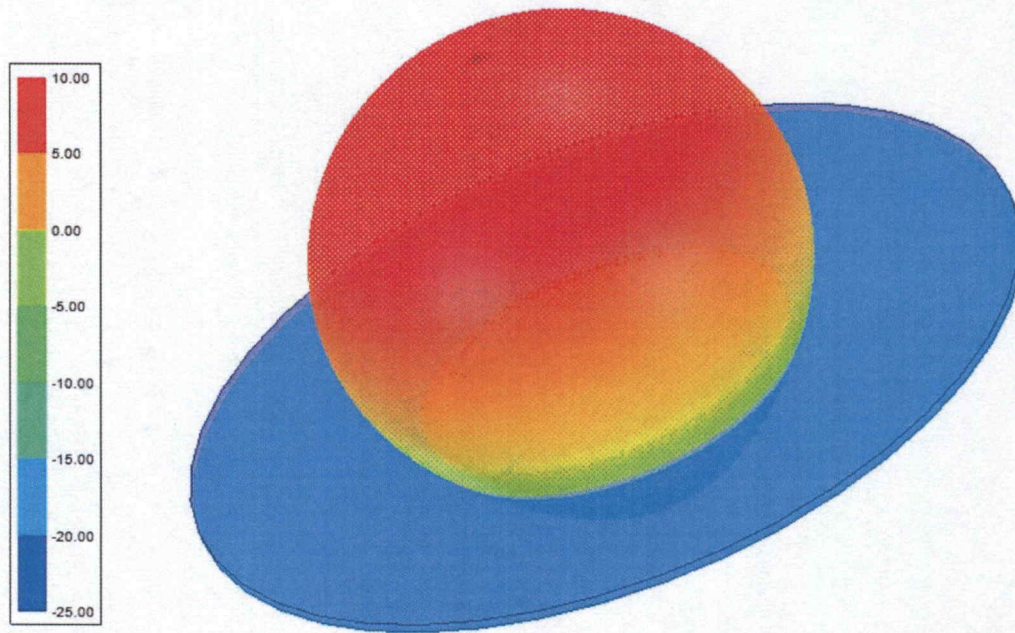
Fig. 5.15: The three-dimensional radiation pattern of the proposed TM_{21} circular patch in Fig. 5.8 of L=6mm and β = 105° at 1.92 GHz.

Table 5.5 compares the unloaded and loaded TM_{12} circular patch antennas. The frequency ratio between the dominant mode and the TM_{12} mode reduces from 2.87 for the unloaded antenna to almost 1.21 for the proposed slit-loaded antenna. The frequency ratio can be set with respect to the needs of the application of the antenna.

Table 5.5: Final comparison between unloaded case and arc slot loaded case for the TM_{12} circular patch antenna

Antenna	Frequency for TM_{12}(GHz)	Frequency for TM_{11}(GHz)	Gain (dBi)	Frequency ratio
Unloaded patch	5	1.74	7.36	2.87
Designed patch in [30]	2.16	1.57	-	1.38
Redesigned patch from [30]	2.06	1.62	9.35	1.27
Proposed arc-loaded patch in Fig. 5.8	**1.92**	**1.58**	**8.08**	**1.21**

5.7 Summary

A dual-band circular patch antenna operating at the TM_{11} and TM_{12} modes was introduced. Two closely-spaced frequencies were realized by placing arc shaped slots with inward radial extensions to elongate the current path associated with the TM_{12} mode, without interfering with the TM_{11} surface currents. A parametric study was conducted to understand the effects of the modified arc slots on the frequency ratio, gain, and reflection coefficients. It was concluded that the resonant frequency of the TM_{12} mode can be controlled by changing the angular opening of the arc and the length of the extensions added to the arc. A frequency ratio as small as 1.21 was achieved, which is smaller than the previously reported frequency ratio of 1.38.

CHAPTER 6

Conclusion and Future Scope

6.1 Conclusion

In this thesis, the miniaturization of circular microstrip patch antennas operating at the higher order modes was investigated to reduce the antenna patch size down to the size of its dominant mode or close to it. This study was motivated by the commercial boom in wireless communications and the need for antennas with conical radiation patterns and dual-band antennas with stable radiation patterns. In general, conventional microstrip patch antennas operating at the higher order modes occupy much larger aperture areas than the dominant mode. Therefore, miniaturized and compact patch antennas at the higher order modes are in demand for the aforementioned applications. In particular, this thesis was focused on miniaturizing the TM_{21} and TM_{31} modes in circular patch antennas, which resulted in conical radiation patterns with aperture areas close to the dominant TM_{11} mode. In addition, miniaturization of the TM_{12} mode was investigated, which resulted in a dual-band antenna with stable broadside radiation patterns. For all these modes, the slit-loading technique in the patch layer was utilized to achieve the miniaturization.

First, a TM_{21} mode circular patch with conical radiation patterns was investigated, whose radius was successfully reduced to that of the dominant TM_{11} mode, which is $0.293\lambda_d$. The miniaturization was realized by placing four radial slits in the maxima of the TM_{21} mode surface current to elongate the current path and thus reduce the aperture size of the antenna. A parametric study was conducted to understand the effects of the slits on

the size reduction, gain, and reflection coefficients. It was concluded that size of the patch can be controlled by changing the radial and angular dimensions of the slits. Reduction up to 40% was achieved in the patch radius, which made its aperture size equal to that of the conventional dominant mode. It is also possible to achieve further miniaturization by modifying the slit geometry. The antenna was fabricated and tested in the spherical near-field anechoic chamber of the University of Alabama in Huntsville. The reflection coefficients and the radiation patterns of the fabricated TM_{21} mode circular patch antenna were in agreement with the full-wave simulation results.

Next, the research was extended to the TM_{31} higher mode in circular patch antennas, generating conical radiation patterns. The slit loading technique was used to elongate the surface currents on the patch, which consequently reduced the resonant frequency of the TM_{31} mode close to that of the TM_{11} mode. Inspired by the surface current distributions of the TM_{31} mode, six radial slits were cut from the patch, which reduced the TM_{31} mode patch radius from $0.668\lambda_d$ to $0.3424\lambda_d$, close to the radius of the dominant mode. Therefore, the new eigenvalue of the TM_{31} circular patch is reduced from 4.20119 to 2.1514. Thus, the original radius and area of the TM_{31} mode patch were reduced up to 49% and 74%, respectively. The radiation patterns and reflection coefficients were thoroughly investigated for different values of the radial opening angle and the length of the slits. The effect of the miniaturization on other modes, including the TM_{11} and TM_{21}, was also numerically studied. It was found that the resonant frequencies of these modes were slightly changed.

Finally, circular patch antennas operating at the TM_{11} and TM_{12} modes were studied for dual-bad applications with stable broadside radiation patterns. Conventional TM_{12}

mode patch antennas not only require larger aperture areas, they also have unwanted sidelobes in the E-plane. To simultaneously address these issues, two mirror-imaged arc slots were symmetrically placed near the disk perimeter to miniaturize the TM_{12} mode without much affecting the dominant mode, and to eliminate the undesired sidelobes at the E-plane, similar to the work reported in [30]. The emphasis was placed on further miniaturizing the TM_{12} mode, without disturbing the dominant TM_{11} mode, and reduce the frequency ratio to as close as unity. To this end, the arc-loaded circular microstrip patch antenna was further investigated by implementing additional radial slots to bring the resonant frequency of the TM_{12} mode closer to that of the TM_{11} mode. The proposed method resulted in a very small frequency ratio of 1.21, outperforming the previously-published paper [30] with the reported ratio of 1.38. Parametric studies were conducted to understand the effects of the arc on the frequency ratio, gain, and reflection coefficients. It was concluded that the frequency ratio can be controlled by changing the opening angle of the arc and the length of the extra radial slots. The width of the arc had negligible impact on the frequency ratio. The realized frequency ratio was 1.21 which is less than the reported ratio of 1.38 from previous research.

This research concludes with new set of eigenvalues to design microstrip circular patch antennas operating at higher modes. These new eigenvalues need not be strictly followed and can be altered with application requirements.

Table 6.1: Summary of new eigenvalues of miniaturized circular patch antennas studied in this thesis

Mode (TM$_{nm}$)	TM$_{21}$	TM$_{31}$	TM$_{12}$
Existing eigenvalues	3.05424	4.20119	5.331
Modified eigenvalues, studied in this thesis	1.841	2.15148	1.917

6.2 FUTURE WORK

Although the basic concept of miniaturized higher order circular microstrip patch antennas has been studied in this thesis using the slit-loading technique for single- and dual-band applications, there are some interesting areas which need further investigation, research, and development, some of which are listed below:

• Development of miniaturized dual-mode circular patch antennas operating at the TM$_{11}$ and TM$_{21}$ modes.

• Fabrication and characterization of the miniaturized TM$_{31}$ patch antenna in the thesis to confirm the numerical results.

• An investigation on miniaturized antennas by coupling the TM$_{1n}$ modes over a wide frequency band.

• A study on miniaturized tri-mode patch antennas operating at the TM$_{11}$, TM$_{21}$, and TM$_{31}$ mode in a single-layer structure.

- Study phased array antennas consisting of miniaturized higher order patch antenna elements.

- An investigation on frequency reconfigurable antennas based on the proposed miniaturized antennas with embedded PIN diodes.

- Validate the numerical results of the proposed dual-band circular patch antenna at the TM_{11} and TM_{12} modes.

REFERENCES

[1] IEEE Standard for Definitions of Terms for Antennas, IEEE Std. 145, 6 March 2014.

[2] C. A. Balanis, *Antenna Theory: Analysis and Design.* 4th edition, Hoboken, NJ, USA: John Wiley & Sons Inc., 2016.

[3] D. M. Pozar, "Microstrip Antennas," *Proc. IEEE*, vol. 80, no.1, pp. 79–91, Jan. 1992.

[4] P. Enge and P. Misra, "Special Issue on Global Positioning System," *Proc. IEEE*, vol. 87, no.1, pp. 3–15, Jan. 1999.

[5] G. A. Deschamps, "Microstrip Microwave Antennas," in the *Third USAF Symp. Antennas,* 1953.

[6] J. Howell, "Microstrip Antennas," *IEEE Trans. Antennas Propag.,* vol. 23, no.1, pp. 90–93, Jan. 1975.

[7] R. Garg, P. Bhatia, I. Bahl, and A. Ittipiboon, *Microstrip Antenna Design Handbook.* Artech House, Norwood MA 1995.

[8] Y. T. Lo, D. Solomon, and W. F. Richards, "Theory and Experiment on Microstrip Antennas," *IEEE Trans. Antennas Propag.*, vol. 27, pp. 137–145, March 1979.

[9] J. Huang, "Circularly Polarized Conical Patterns from Circular Microstrip Antennas," *IEEE Trans. Antennas Propag.*, vol. 32, pp. 991–994, Sept. 1984.

[10] H. A Wheeler, "Fundamental Limitations of Small Antennas," *Proc. IRE*, vol. 35, pp. 1479–1484, Dec. 1947.

[11] L. J. Chu, "Physical Limitation on Omni-Directional Antennas," *J. Applied Physics*, vol. 19, pp. 1163–1175, Dec. 1948.

[12] J. S. McLean, "A Re-Examination of the Fundamental Limits on the Radiation Q of Electrically Small Antennas," *IEEE Trans. Antennas Propag.*, vol. 44, pp. 672–675, May 1996.

[13] R. E. Collin and S. Rothschild, "Evaluation of Antenna Q," *IEEE Trans. Antennas Propag.*, vol. 12, pp. 23–27, Jan. 1964.

[14] R. L. Fante, "Quality Factor of General Ideal Antennas," *IEEE Trans. Antennas Propag.*, vol. 17, pp. 151–155, March 1969.

[15] R. F. Harrington, "Effect of Antenna Size on Gain, Bandwidth and Efficiency," *J. Research of the National Bureau of Standards - D. Radio Propag.*, ser. D vol. 64, pp. 1–12, Jan. –Feb. 1960.

[16] K. Fujimoto, A. Henderson, K. Hirasawa, and J. R. James, *Small Antennas*. New York, John Wiley and Sons, Research Studies Press, 1987.

[17] O. Staub, J.-F. Zurcher, and A. Skrivervik, "Some Considerations on the Correct Measurement of the Gain and Bandwidth of Electrically Small Antennas," *Microw. Optical Technol. Lett.*, vol. 17, no. 3, pp. 156–160, Feb. 1998.

[18] M. Lee, C.-C. Chen, and J. L. Volakis, "Ultra-Wideband Antenna Miniaturization using Distributed Lumped Element Loading," *IEEE Antennas Propag. Society Int. Symp.*, Washington, DC, USA, 3–8 July 2005.

[19] J. Kula, D. Psychoudakis, W. J. Liao, C.-C. Chen, J. Volakis, and J. Halloran, "Patch Antenna Miniaturization using Recently Available Ceramic Substrates," *IEEE Antennas Propag. Mag.*, vol. 48, pp. 13–20, Dec. 2006.

[20] H.-M. Chen, Y.-K. Wang, Y.-F. Lin, C.-Y. Lin, and S.-C. Pan, "Microstrip-Fed Circularly Polarized Square-Ring Patch Antenna for GPS Applications," *IEEE Trans. Antennas Propag.*, vol. 57, no. 4, pp. 1264–1267,Apr. 2009.

[21] P. M. T. Ikonen, K. N. Rozanov, A. V. Osipov, P. Alitalo, and S. A. Tretyakov, "Magnetodielectric Substrates in Antenna Miniaturization Potential and Limitations," *IEEE Trans. Antennas Propag.*, vol. 54, pp. 3391–3399, Nov. 2006.

[22] R. Pascaud, H. Legay, and T. Calmettes, "Compact Dual-Polarized VHF Microstrip Patch Antenna for Satellite Applications," in the *15th Int. Symp. Antenna Technol. Applied Electromagnetics (ANTEM),* Toulouse, France, June 25–28, 2012.

[23] R. Waterhouse, "Small Microstrip patch antenna", *Electronic Lett.*, vol. 31, pp. 604–605, 1995.

[24] C. B. Ravipati, D. R. Jackson, and H. Xu, "Center-Fed Microstrip Antennas with Shorting Vias for Miniaturization," in the *Int. Symp. IEEE Antennas Propag. Society*, vol. 3B, Washington, DC, USA, pp. 281–284, July 2005.

[25] Rogers Corporation, "RT/duroid 5870/5880 High Frequency Laminates," 5870/5880 datasheet, [Revised June 2017].

[26] S. Naik and M. Pour, "A Miniaturized TM_{21} Mode Circular Microstrip Patch Antenna", *Progress In Electromagnetics Research Lett.,* in press, 2019.

[27] High Frequency Structure Simulator (HFSS 18.0). Canonsburg, PA, Boston, MA: ANSYS. [Online]. Available: http://www.ansoft.com/products/hf/hfss.

[28] S. Maci and G. Biffi Gentili, "Dual-Frequency Patch Antennas," *IEEE Antennas Propag. Mag.*, vol. 39, no. 6, pp. 13–20, Dec. 1997.

[29] S. Maci, G. Biffi Gentili, P. Piazzesi, and C. Salvador, "Dual-Band Slot-Loaded Patch Antenna," *IEE Proc.-Microw. Antennas Propag.*, vol. 142, no. 3, pp. 225–232, June 1995.

[30] K.-L. Wong and G.-B. Hsieh, "Dual-Frequency Circular Microstrip Antenna with a Pair of Arc-Shaped Slots," *Microw. Optical Technol. Lett.*, vol. 19, no. 6, pp. 410–412, Dec. 1998.

[31] G. B. Hsieh and K. L. Wong, "Inset Microstrip Line Fed Dual-Frequency Circular Microstrip Antenna and its Application to a Two-Element Dual-Frequency Microstrip Array," *IEE Proc.-Microw. Antennas Propag.,* vol. 146, no. 5, pp. 359–361, Oct. 1999.